C.P. No. 766

C.P. No. 766

MINISTRY OF AVIATION

AERONAUTICAL RESEARCH COUNCIL

CURRENT PAPERS

Annular Cascade Experimental Investigations of Conical Actuator Disc Theory and of Non-Uniform Flow through Plane Walled Diverging or Converging Ducts

By

R I. Lewis,

English Electric Co. Ltd.

LONDON· HER MAJESTY'S STATIONERY OFFICE

1965

PRICE 8s. 6d. NET

C. P. No.766

Annular Cascade Experimental Investigations of Conical
Actuator Disc Theory and of Non-Uniform Flow through
Plane Walled Diverging or Converging Ducts
- By -
R. I. Lewis,
English Electric Co. Ltd.

Communicated by Dr. D. S. Whitehead

October, 1963

SUMMARY

A description is given of wind tunnel experimental investigations
of rotational flows through diffusers and contractions. The purpose of the
investigations was to test the accuracy of a theory previously derived for
two-dimensional plane walled diverging or converging ducts and of actuator
disc theory for conical annuli. Conical flow tests were made in one case
with a free vortex blade row of large deflection. Other tests were made
with an axial compressor inlet guide vane nozzle generating a small
swirling velocity distribution close to solid rotation. Particular
attention is drawn to the separate influences exerted by two vorticity
components originating from gradients of stagnation pressure and of fluid
angular momentum.

List/

List of Contents

1. Introduction

The fluid dynamic design of an axial turbo-machine requires the solution of three main problems. In the first stage the energy transfer process between the working fluid and the rotor is specified for each streamline. This involves the specification of stagnation pressure or enthalpy along each streamline and in consequence the distribution of fluid angular momentum. It is necessary here to assume a streamline pattern. For example, the potential flow streamline distribution which can be computed for the annulus with the blades removed is usually taken as the starting point.

In the second design stage the centrifugal balance of the fluid is calculated for the specified distributions of stagnation pressure and fluid angular momentum. If gradients of these quantities exist normal to the assumed axisymmetric potential flow surfaces, the flow is in fact rotational. The stream surfaces of revolution then depart slightly from the potential flow surfaces computed in Stage No.1. The velocities thus calculated are of second order of accuracy for first order rotational perturbations which is quite good enough for practical purposes. If, on the other hand, gradients of stagnation pressure and fluid angular momentum are zero normal to the stream surfaces of revolution, the flow is irrotational and design Stage No.2 is not required. Among the available analyses the most successful for axial flow machines are radial equilibrium[1], actuator disc[2] and single parameter[9] theories. With these theories it is possible to estimate the axial velocity profiles which for all cases except the rotational or free vortex case, are non-uniform. With this information it is then possible to construct the correct velocity triangles.

The third design stage consists of the selection of blade cascades which are aerodynamically suitable for producing the correct velocity triangles.

This paper is concerned mainly with experimental investigations of the radial balance of swirling fluids in conical annuli, in connection with the second design stage. The development of actuator disc theory for cylindrical annuli[2] can be traced through Refs.3 to 7. A fair volume of supporting experimental work has been undertaken in parallel which has shown the accuracy of the theory, for example, Refs.8 and 9. The present project has been concerned with the extension of actuator disc theory to non-cylindrical ducts. As a first step the flow through two-dimensional plane walled diverging ducts was considered[11] and also the non-swirling flow through conical annuli. These systems correspond to the flow from line and point sources, respectively, with the introduction of rotational velocity perturbations. The conical theory was then extended to include swirling velocity components and a conical actuator disc theory was developed[12]. In parallel with these theoretical studies the present paper sets out to present an experimental investigation of both stages of development of the theory. Section 3 describes the two-dimensional plane walled duct experiments. Sections 4 and 5 describe various conical duct experiments designed to bring out some of the more interesting results of the theory. In particular, these experiments have been arranged to illustrate the two types of vorticity which are found in incompressible flow arising from gradients of stagnation pressure and fluid angular momentum normal to the stream.

In the section which follows, some of the fundamental background theory is given. Equations giving the actual theoretical predictions in terms of the experimental duct geometries are included in each section for reference as well as for illustrative purposes. The detailed derivation of some of these equations is included in Appendix II.

2. Fundamental Background

The fluid is assumed to be inviscid and incompressible. The further assumption is made that the flow is axisymmetric, for which case the continuity equation may be written in cylindrical co-ordinates Z, R, θ, Fig.1 as follows:

$$\frac{\partial u}{\partial Z}$$

- 4 -

$$\frac{\partial u}{\partial Z} + \frac{\partial v}{\partial R} + \frac{v}{R} = 0 . \qquad \qquad \ldots (1)$$

From this equation Stokes' stream function ψ may be defined such that

$$uR = -\frac{\partial \psi}{\partial R} \left. \vphantom{\begin{array}{c}1\\1\\1\end{array}} \right\} \qquad \qquad \ldots (2)$$
$$vR = \frac{\partial \psi}{\partial Z} . $$

The tangential (θ) component of vorticity is defined as

$$\eta = \frac{\partial v}{\partial Z} - \frac{\partial u}{\partial R} \qquad \qquad \ldots (3)$$

which, on substitution from (2), gives an equation relating ψ to η

$$\frac{\partial^2 \psi}{\partial R^2} - \frac{1}{R} \frac{\partial \psi}{\partial R} + \frac{\partial^2 \psi}{\partial Z^2} = \eta R . \qquad \qquad \ldots (4)$$

Also since ψ is a function of R and Z only

$$\frac{d\psi}{dt} = \frac{\partial \psi}{\partial R} . \frac{dR}{dt} + \frac{\partial \psi}{\partial Z} . \frac{dZ}{dt}$$

or for steady flow using equations (2)

$$v \frac{\partial \psi}{\partial R} + u \frac{\partial \psi}{\partial Z} = 0 . \qquad \qquad \ldots (5)$$

In vector notation we have

$$q . \text{grad } \psi = 0 \qquad \qquad \ldots (5a)$$

which states that the gradient of ψ is normal to the velocity in the Z, R plane. In other words ψ is constant along each streamline.

It is possible to deduce also[4,13] from the equations of motion and easy to visualise that in the absence of blade forces the fluid total pressure p_0 and angular momentum about the axis (wR) will both be conserved along streamlines.

$p_0/$

$$p_o = f_1 (\psi)$$

$$\ldots (6)$$

$$wR = f_2 (\psi) .$$

Another important equation, derived by Bragg and Hawthorne[4] relates η to p_o and (wR)

$$\eta = w \frac{d(wR)}{d\psi} - \frac{R}{\rho} \frac{dp_o}{d\psi} . \qquad \ldots (7)$$

All of these derivations are dealt with in more detail in Ref.13.

Equation (7) states that gradients of (wR) and p_o normal to the streamlines correspond to the existence of two components of the tangential vorticity η. It has also been shown in Ref.13 that these components are quite distinct from one another. The first is known as streamwise vorticity and originates from the shedding of blade bound vorticity into the stream with the vector direction of the velocity. This vorticity resolves into axial, radial and tangential components. The second component of η, due to gradients of p_o, is known as smoke-ring vorticity because it forms closed rings concentric with the machine axis. The streamwise and smoke-ring vorticities are illustrated in Fig.2.

If derivatives of p_o and (wR) normal to the streamlines are zero, η is zero also and the flow is irrotational as mentioned in the introduction.

Equations (6) and (7) may now be combined to give

$$\eta = \frac{F_1 (\psi)}{R} + RF_2 (\psi) \qquad \ldots (8)$$

where F_1 and F_2 are functions of ψ and are related to derivatives of (wR) and p_o.

It is evident from equation (8) that for converging or diverging flows in which R varies following each streamline, the streamwise and smoke-ring tangential vorticities will vary differentially. One will increase in strength in proportion to R while the other will decrease inversely with R. In the case of cylindrical flow this result has no significance. The conical theory and experiments have been conceived for the purpose of illustrating this result for the simplest known diverging flow namely that of a rotational source flow. The smoke-ring and streamwise vortex filaments are convected along surfaces which are almost conical and produce a known variation of R. The detailed analytical results are derived in Refs.11 and 12 and summarised in Ref.13.

Smoke-ring vorticity has been introduced by using suitable gauzes to generate variations of p_o. Streamwise vorticity has been generated by the introduction of annular cascades of blades. Experimental details are included in each section.

3. **Two-Dimensional Experiments with Plane Walled Diffusers and Contractions**

The experiments described in this section were conducted with plane walled diffusers and contractions illustrated in Fig.3. The purpose of the tests was to investigate the effect of duct divergence or convergence upon velocity profiles generated by gradients of stagnation pressure. In this

case a vorticity component is present normal to the two-dimensional plane
and similar to the smoke-ring vorticity found in axisymmetric flow. In the
presence of this vorticity it has been shown[11] that inlet and outlet axial
velocity perturbations u', that is departures from the irrotational
velocity U, for each streamline are related by the equation

$$\frac{u_2'}{U_2} = \lambda^2 \frac{u_1'}{U_1} \qquad \qquad \dots (9)$$

where
$$\lambda = \frac{\text{outlet area}}{\text{inlet area}} \ .$$

3.1 Description of rig

A special working section, shown in Fig.3, was built into the
10 in. × 5 in. low speed wind tunnel at the Cambridge University Engineering
Laboratory. The duct was in two sections of constant depth 10 in. The first
section was 12 in. in length and had parallel side walls 5 in. apart. The
side walls of the second section continued parallel for a further length of
16 in. and then merged through a short flexible length of perspex into
another plane walled section of variable divergence angle θ_1. The duct
ejected into the room.

Pitot traverses were made at entry into the diverging section,
Station 1, and at outlet, Station 2. Two static pressure tappings were
provided just upstream of Station 1, in the top wall. Another tapping was
provided in Section 1 which, in combination with a total pressure probe
inserted in the same plane, gave a mass flow calibration uninfluenced by
changes of Section 2 or by gauzes introduced between Sections 1 and 2.

Pitot static measurements were made at Station 2. At Station 1
total pressure probe readings were combined with static pressure recorded
at the wall, in order to compute inlet velocity.

3.2 Preliminary tests

An initial test was made with a narrow gauze strip generating a
strongly sheared profile and with parallel walls, in order to check
whether or not significant viscous diffusion of the vorticity of the
sheared profile was likely to take place. Velocity profiles at Stations 1
and 2 are shown in Fig.4a. It is apparent that little change in the
velocity profile occurred between inlet and outlet.

The duct angle was then increased to 15° of diffusion. Resulting
inlet and outlet velocity profiles are shown in Fig.4b.

The dashed curve is the theoretical outlet velocity predicted from
the inlet velocity profile by equation (9). The area ratio was 1·47.

Further tests with this gauze were abandoned because of flow
separations in the low velocity regions at the centre of the top and bottom
walls, which distorted the two-dimensional pattern of the flow. Small
separation zones were present in the test described. Even so, close agreement
was obtained with the theoretical prediction. Maximum perturbations were as
great as 40%.

This preliminary test did indicate that a concave velocity
distribution inhibits flow separation from the diverging walls of a plane
diffuser to a marked degree. The duct angle was increased to 20° before any
large scale stalling occurred, except of course in the low velocity regions on
the top and bottom walls where reasonably steady separation zones were found.

3.3 Linear velocity profile

A linear shear profile was generated by an array of $\frac{1}{8}$ in. diameter steel rods set at a graded spacing. With this profile the flow separated from the diverging wall on the low velocity side even for small angles of divergence. One experiment was completed with 10° of convergence and with an area ratio of 0·7. Inlet and outlet velocity profiles are compared in Fig.5 with a theoretical linear shear profile ignoring boundary layers. Extremely close agreement was obtained for the main stream velocity.

3.4 Concave velocity profiles

More detailed tests were made using gauzes 1 and 2, Fig.3, which were shaped to generate concave velocity profiles with small perturbations to restrict the separation zones on the top and bottom walls.

Detailed surveys of the inlet velocity profiles were made at Station 1, Figs.6a and 6b. Similar traverses were made at various duct depths which revealed that the inlet velocity variations were approximately two dimensional. Gauze No.2 had slightly better characteristics than gauze No.1 in this respect. With gauze No.2, detailed traverses were also made at outlet revealing equally good two-dimensional conditions at outlet, Fig.6c.

Gauze No.1

With this gauze measurements were made of the outlet velocity profile with 10° of divergence and an area ratio of 1·3 and also with 10° of convergence and an area ratio of 0·67. Results compared closely with equation (9) for both tests, Fig.7. It can be seen that perturbations are increased in magnitude by diffuser and attenuated by a contraction.

Gauze No.2

In Fig.8 one comparison only is given of the theoretical and experimental outlet velocity profiles with a divergence of 12·1°. Agreement was very good, the worst errors occurring in the low velocity region. It is always the case that the linearised theory over-predicts the perturbation (compare Figs.4, 7 and 8).

4. Annular Cascade Experiments for Conical Flow

The annular cascade experiments to be described now were modelled on conical actuator disc theory. As already mentioned a point source flow is taken as the basic irrotational flow system in the absence of blade rows. When working in spherical co-ordinates it is convenient then to take, as hub and casing, cones with a common vertex located at the source. Inlet and outlet areas are spheres of radius r_1 and r_2, Fig.1. In the theory[12] the fluid is assumed to be in radial equilibrium, that is cylindrical flow, at r_1 and r_2, when swirling velocities are present. In the absence of swirl, constant static pressure is assumed to exist at r_1 or r_2. For experimental purposes short cylindrical lengths were provided at inlet to and outlet from the conical working section.

A detailed description of the annular cascade wind tunnel has been given in Ref.15. The rig is shown in Fig.9 and in cross section in Fig.10. The main components are the Borda inlet contraction, working section, outlet section and diffuser. The rig is located on the inlet orifice of a

centrifugal/

centrifugal fan and operates as a suction tunnel receiving air from the
laboratory with constant stagnation pressure equal to room pressure.
Gradients of stagnation pressure were obtained by suspending suitably shaped
gauzes in the inlet contraction.

The working section consists of an accurately bored frame in
which components such as blade rings, traversing rings or shaped casings can
be housed. These are then free to rotate if circumferential traverses are
required. The conical duct assembly including a blade row is shown
diagrammatically in Fig.10.

The tests which are to be described may be summarised as follows:

(i)   Flows without swirl, but with gradients of
       stagnation pressure.

(ii)   Flows with small swirling components, with
       and without gradients of stagnation
       pressure.

(iii) Flows with a free vortex cascade of large
       deflection with and without gradients of
       stagnation pressure.

(iv)   Flows with a solid rotation cascade of small
       deflection with and without gradients of
       stagnation pressure.

4.1 Conical flow without swirl

The duct used for the non-swirling test, Fig.11a, was contracted
in diameter from 14 in. to 10·76 in. through a cone of total angle 20° 24'
and with an area ratio of 0·59. This was preceded by a cylindrical section
$5\frac{1}{2}$ in. long and followed by a cylindrical outlet section 15 in. long.
Traversing stations are also shown in Fig.11a. Total and static pressures
were measured by means of a wedge probe described in Ref.15. This probe was
found to be subject to smaller calibration errors near to the walls than the
cylindrical probe of more conventional usage.

4.1.1 Uniform total pressure

As previously mentioned, constant static pressure is assumed to
prevail at r_1 and r_2. In these experiments it was not possible to arrange
these boundary conditions exactly because the unperturbed irrotational flow
pattern upstream of r_1 and downstream of r_2 was not that of a point source,
but of a source flow merged into a cylindrical flow. In consequence, slight
static pressure gradients were found at stations 1 and 2 in the sense that one
would expect for the merging regions. A test was made with constant inlet
stagnation pressure to investigate these effects, Fig.12.

The plots of static pressure and velocity shown in Fig.12 are
slightly distorted by calibration errors near to the wall through which the
probe was inserted. The dashed curves show an estimate of the true static
pressure.

This test suggested that the boundary conditions were close to those
assumed theoretically.

4.1.2 Stagnation pressure gradient

The experimental procedure was repeated with non-uniform stagnation
pressure generated by a conical shaped gauze, with a 60° vertex angle,
suspended in the inlet contraction in the manner illustrated in Fig.10. A
concave axisymmetric velocity profile was generated with this arrangement,

Fig.13. The dashed curve shows the theoretical outlet profile according to equation (9), compared with that recorded experimentally. Agreement was very close indeed. The maximum perturbation was attenuated from about 20% to 7% through this contraction. Similar small variations of static pressure across the duct were recorded as for the previous experiment. For the purpose of computing velocity, recorded total pressure was combined with the mean value of static pressure.

4.2 Conical flow with small swirling velocities

For this experiment the same casing was used, Fig.11b, but a conical hub of common vortex was introduced, having a total angle of 9° 40'. Swirling velocities were introduced by means of a row of compressor inlet guide vanes designed to generate a vortex near to solid rotation. For this experiment however the stagger was set 5° less than design to reduce the magnitude of the swirling velocities. The hub was located centrally by the blades at one end and by three struts, set mutually at 120°, downstream of the working section. The traversing stations are also shown in Fig.11b. Mean readings over one circumferential blade pitch were taken of swirl angle, static pressure and total pressure using the wedge probe.

A gradient of stagnation pressure at Station 1, Fig.14, was generated by means of the conical gauze. In this way smoke-ring vorticity was introduced upstream of the inlet guide vanes. Streamwise vorticity of similar magnitude was also shed from the blade trailing edges, so that both components were present in the duct.

The axial velocity profiles at Stations 1 and 2 are shown in Fig.15a. The shear rate was almost linear and quite large. Since the flow was almost axial, the tangential component of the streamwise vorticity was very small compared with the smoke-ring vorticity. The theoretical outlet profile shown in Fig.15 has therefore been computed from equation (9) neglecting the streamwise vorticity. The theory predicts the outlet profile quite adequately.

The swirl velocity, shown in Fig.15b, also compares well with the solution derived in Ref.12 which simply expresses that angular momentum (wR) is conserved approximately along unperturbed stream surfaces, that is conical surfaces:

$$ w'r \doteqdot f(\theta) . \qquad \qquad \qquad \dots (10) $$

Excellent agreement between theory and experiment has been obtained for small swirling flows on this basis. The swirl angles here had a maximum value of 22° at the casing, with the result that tangential components of the streamwise vorticity were so small as hardly to affect the axial velocity profile.

4.3 Conical annular flows with large free vortex and perturbed free vortex swirl

The experiments described in this section were conducted with the annulus used for the small swirl experiments, Section 4.2, but with a free vortex blade row of large deflection introduced half-way along the annulus. Experiments were made with and without gradients of inlet stagnation pressure.

A cross sectional view of the conical duct assembly used for the experiments is shown in Fig.10. The duct under consideration is bounded by the conical hub and casing and by planes perpendicular to the axis at r_1 and r_2. The mathematical model requires spherical inlet and outlet boundaries r_1 and r_2. Planes were chosen to simplify the traversing arrangements. In fact the traversing planes 1 and 4 were placed within the cylindrical inlet and outlet lengths where radial equilibrium was assumed

to exist in accordance with the theoretical requirements for r_1 and r_2.
In other words the fluid was assumed to achieve radial equilibrium at
r_1 and r_2 and to continue in radial equilibrium to Stations 1 and 4.

Experiments were made with both converging and diverging ducts
although only the converging assembly is shown in Fig.10. For these
experiments a free vortex nozzle blade row was located half-way along the
conical section. The same conical section was used as for the small
swirling tests, with additional traversing Stations 2 and 3 located at
approximately one quarter of a blade chord upstream and downstream of the
blades. It was also possible to make circumferential traverses at other
positions by allowing the conical sections to rotate with the probe. At
Stations 1 to 4 special traversing rings were provided.

The two conical sections, separated by the blade ring, were made
of perspex to permit the use of flow visualisation techniques. Another
advantage was found in the simplicity with which the probe could be set
visually to zero at the casing.

4.3.1   Test No.1 - Converging duct with constant total pressure inflow

In the first test air entered the duct with constant total
pressure equal to atmospheric pressure. The hub and casing boundary layers
at Stations 1 and 2 are shown in Fig.1b. Although the main stream inflow
was irrotational, there was a considerable variation of static pressure and
velocity at Station 1, from hub to casing, Fig.17. It was found to be
possible to modify the theory given in Ref.12 to take this static pressure
gradient into consideration.

The traverse at Station 2 just upstream of the blades, Fig.17,
showed that static pressure and velocity were almost constant. This is
in accordance with expectations for a point source free vortex flow, for
which the axial velocity U is constant at radius r

$$u = \frac{C}{r^2}.$$

The value of r would vary but little for the actual plane of
traverse because of the narrow angle of the duct.

Conditions at the blade row were thus ideal for the generation
of a free vortex conical flow.

The swirl angles measured at Station 3 are compared in Fig.18
with the design angles for cylindrical flow at the same radii. It is of
particular interest that blades designed from two-dimensional cascade
data[15,16] should produce the same swirl angles in a three-dimensional
conical flow in which the angle of intersection of the conical stream
surfaces and the plane of the cascade varied from approximately 80° to 85°.

Fig.19 shows the axial and swirling velocity components U and
w at Stations 3 and 4 in comparison with predicted values assuming the
design potential conical free-vortex given by

$$U = \frac{C}{r^2} \qquad\qquad w = \frac{K}{r \sin \theta} \qquad\qquad \dots (11)$$

$$= \frac{K}{R}$$

where C and K are constants.

It/

It is much to the credit of the cascade data that the design swirl velocity was obtained to within $1\frac{1}{2}\%$. Rather larger axial velocity variations occurred due to secondary flow effects. The secondary vorticity, however, exercised little influence upon the swirling velocity.

At Station 4 a very thick hub boundary layer had grown. This is thought not to have been due to normal growth, but rather to the accumulation of low energy air from the blade wakes centrifuged under the strong radial pressure gradient imposed by the large swirling velocities. Outside the boundary layer regions the flow compared well with the conical free vortex at Station 4 also, Fig.19. The axial velocity was almost uniform but increased by the blockage resulting from the thick hub boundary layer. The swirling velocity remained close to a free vortex swirl.

From this test with irrotational inflow some idea has been obtained of the possible extent to which viscous effects were likely to have affected Test No.2 with rotational inflow conditions. Outside the boundary layer regions good agreement with the inviscid theory is to be expected.

4.3.2 Test No.2 – Converging duct with non-uniform inlet stagnation pressure

The experimental procedure of Test No.1 was repeated with the conical gauze fixed in the inlet contraction to generate a gradient of stagnation pressure p_o. The distributions of p_o at Stations 1, 2, 3 and 4 are shown in Fig.20. The full curve (a) showing the distribution at Station 1 has been superimposed upon the others for comparison. According to approximate conical actuator disc theory[12] p_o is a function of θ only. At Station 2 there was little change from the distribution of p_o at Station 1. Just downstream of the cascade at Station 3, the total pressure was reduced by the blade wake losses. This reduction was greatest near to the hub where the blade passages were long and narrow and the mass flow per unit blade height was least. Also an inward flow of the blade boundary layer under the radial pressure gradient probably tended to increase the losses near to the hub. At Station 4 the growth of a thick hub boundary layer considerably modified the distribution of p_o near to the hub although the distribution was substantially the same over most of the duct area.

The mean static pressure was combined with measured total pressure to compute the axial velocity at Station 1. A linear curve, Fig.21, has been drawn through the experimental points to be used for making theoretical predictions. Velocity components at the other stations have been computed for this inlet velocity profile, assuming the cascade to be replaced by an equivalent actuator disc placed (a) at the mid-chord position, and (b) at the blade trailing edges. In applying the theory the design cascade deflection angles were assumed, Fig.18.

The experimental and theoretical velocity components at Stations 2, 3 and 4 are compared in Figs.21 and 22. Apart from the hub boundary layer and the profile distortion introduced by secondary vorticity, excellent predictions were obtained by the linearised conical actuator disc theory.

An interesting feature of this experiment was the inversion of the axial velocity profile between inlet and outlet. For example, in the absence of swirl the predicted outlet profile, as shown in Fig.21, would have vorticity of the same sign but reduced in magnitude. Thus the law for smoke-ring vorticity would apply

$$\eta_2'' = \left(\frac{r_2}{r_1}\right)^2 \eta_1'' \, . \qquad \qquad \ldots (12)$$

Double and treble primes denote smoke-ring and streamwise vorticities respectively.

With free-vortex blades present, however, the theoretical outlet velocity distribution as derived in Appendix II is

$$\frac{\partial u_2'}{\partial \theta} = \left(\frac{r_2}{r_1}\right)^2 \frac{\partial u_1'}{\partial \theta} - \left\{ \frac{\left(\frac{r_m}{r_1}\right)^2 \tan^2 \alpha}{1 + \frac{1}{2} \tan^2 \alpha} \right\} \frac{u_1'}{\partial \theta} \qquad \ldots (13)$$

Since the fluid is in radial equilibrium the vorticities at inlet and outlet are then related as follows

$$\eta_2 = \left(\frac{r_2}{r_1}\right)^2 \eta_1 - \left\{ \frac{\left(\frac{r_m}{r_1}\right)^2 \tan^2 \alpha}{1 + \frac{1}{2} \tan^2 \alpha} \right\} \eta_1 \qquad \ldots (14)$$

η_2 has two components of opposite sign. One of these is the smoke-ring vorticity admitted at inlet which obeys equation (9) above, just as it would in the absence of the cascade. The other component is the tangentially resolved component of the streamwise vorticity shed from the cascade because of the initial presence of smoke-ring vorticity. The streamwise component

$$\eta_2'' = - \left\{ \frac{\left(\frac{r_m}{r_1}\right)^2 \tan^2 \alpha}{1 + \frac{1}{2} \tan^2 \alpha} \right\} \eta_1 \qquad \ldots (15)$$

is opposite in sign to η_2''. Furthermore, while smoke-ring vorticity is attenuated by a contraction, streamwise vorticity is increased in strength. Consequently, as the fluid proceeds along the duct the weak streamwise vorticity introduced at the cascade grows until finally it dominates the smoke-ring vorticity, causing the inversion of the axial velocity profile at outlet. It is an interesting fact that the streamwise vorticity, while owing its origin to the smoke-ring vorticity, finally dominates at outlet.

It may also be seen from the equations above that the axial position of the actuator disc is a controlling parameter for determining the relative magnitudes of the vorticity components. As the cascade is moved towards inlet (increasing r_m/r_1), the streamwise vorticity has increasing predominance. It would be possible to find a position such that the two components almost cancel one another at outlet resulting in almost zero tangential vorticity and uniform axial velocity. Predictions with the actuator disc at the mid-chord or trailing edge positions, however, were almost identical.

The swirling velocity agreed quite well with the perturbed free vortex predicted.

The greater curvature of the experimental profile at Station 2 than the predicted profile may indicate that the equivalent actuator disc was in fact not parallel to the traversing plane.

The swirl angles at Station 3 have been compared in Fig.18 with those recorded in Test No.1. There was negligible difference between the two,

demonstrating/

demonstrating that secondary flows, due to the deflection of the main stream vorticity, were negligible.

Similar tests were made with the duct reversed. The resulting diffusion gave rise to severe boundary layer growth, although flow separations were restricted to a thin layer on the hub downstream of the blades. Poor agreement with inviscid theory was obtained, although the trends were observed. These experiments are reported in detail in Ref.14. Space does not permit their inclusion here.

5. Conical Annular Flows with Swirling Velocities Close to Solid Rotation

The experiments just described were concerned with flows with large swirling velocities close to a free vortex. The actuator disc theory used for comparison is equally valid for arbitrary swirl distributions provided the induced axial velocity perturbations do not exceed the magnitude permitted by the linearising assumptions.

With irrotational inflow, the flow remains irrotational downstream of the free-vortex cascade because of the constancy of bound circulation along the blade length. The introduction of smoke-ring vorticity at inlet to the duct in the previous experiment caused a change in bound circulation and, in consequence, the shedding of trailing vortex sheets from the blade trailing edges, treated analytically as distributed streamwise vorticity.

With other types of cascade, the blade circulation is intentionally chosen to vary along the blade length. The streamwise vorticity then shed into the stream determines the type of vortex swirl which is generated. For a solid rotation swirl, only restricted deflection angles are permissible to avoid large axial velocity perturbations. For the experiments described here the compressor inlet guide vane row was used, which has swirl angles, measured from the axial direction which ranged from about 10° at the hub to 24° at the casing. The presence of smoke-ring vorticity in the stream, as for the free vortex blade row, causes the shedding of additional streamwise vorticity at the cascade. For these small deflections, however, the tangential component of this small additional streamwise vorticity is quite negligible. It is then sufficiently accurate to superimpose the individual effects of the smoke-ring vorticity with the cascade removed and the streamwise vorticity which would appear in the absence of the smoke-ring vorticity at inlet.

The duct geometry was identical to that for the free vortex tests. Tests were conducted with uniform and non-uniform inlet stagnation pressure as before.

5.1 Uniform inlet stagnation pressure

The swirl angles measured at Station 3, Fig.10, are shown in Fig.23a. By applying the correction for conical flow described in Appendix III it was possible to estimate the swirl angles at the plane of the actuator disc. The tangent of this angle also is shown in Fig.23b with a theoretical curve which represents $\tan \alpha_m$ quite closely, given by

$$\tan \alpha_m = 3 \cdot 30 - 0 \cdot 128.$$

The actuator disc was placed at a distance of one third of the blade chord from the leading edge.

In evaluating the test results an estimate has been made in these experiments of the effects of inlet static pressure gradients. With constant inlet stagnation pressure the inlet static pressure and velocity distributions are shown in Fig.24. The velocity profile was almost linear and of the same order of magnitude as the rotational perturbations induced within the duct, Fig.25. The theoretical outlet velocity profile u'_2/U_2 as derived in Appendix II is as follows:

$$\frac{u'_2}{U_2}$$

$$\frac{u_2'}{U_2} = \frac{1}{K_1}\left(\frac{r_2}{r_m}\right)^2\left\{\frac{K_2}{\left[\dfrac{2}{K_1} + \tan^2\alpha_m\right]^2} - 1\right\} \qquad \ldots (16)$$

where

$$K_1 = \left[1 + 2\frac{u'}{u_2'}\left(\frac{r_1}{r_m}\right)^{n-1}\right].$$

In Test No.1 K_1 had a value of 1·054 compared with unity for the case of constant inlet static pressure. The resulting theoretical velocity profile at outlet is compared in Table I with that for constant inlet static pressure.

Table 1

$\dfrac{\theta - \theta_1}{\theta_2 - \theta_1}$		0	0·2	0·4	0·6	0·8	1·0
$\dfrac{u_2'}{U_2}$	Theory A	0·05137	0·03799	0·02075	0·00000	-0·02337	-0·04923
	Theory B	0·05141	0·03798	0·02072	0·00000	-0·02328	-0·04892

The similarity between these two predictions shows that the inlet pressure variations decayed to sufficiently small proportions to ensure that the change in streamwise vorticity shed from the actuator disc was negligible. The axial velocity within the duct may then be adequately predicted by superimposing the effect of the inlet pressure gradient upon the solution calculated for constant inlet static pressure.

Thus we have, upstream of the actuator disc

$$u' = u_1'\left(\frac{r}{r_1}\right)^{n-1} + \frac{1}{2}\left(\frac{r_m}{r}\right)^{n+2}u_2' \qquad \ldots (17a)$$

and downstream of the disc

$$u' = u_1'\left(\frac{r}{r_1}\right)^{n-1} + \left[1 - \frac{1}{2}\left(\frac{r}{r_m}\right)^{n+2}\right]u_2' \qquad \ldots (17b)$$

where

$$\frac{u_2'}{U_2} = \left(\frac{r_2}{r_m}\right)^2\left\{\frac{K}{\left[2 + \tan^2\alpha_m\right]^2} - 1\right\}. \qquad \ldots (18)$$

To illustrate the influence of the inlet static pressure gradient, the mean shear rate of the axial velocity perturbation profile has been shown in Fig.25 as a function of position along the duct. The full curve shows that

according to Theory A the perturbations at the actuator disc reach half of
their final value at outlet. The dashed curve, Theory B, on the other
hand illustrates the manner in which the inlet static pressure perturbation
attenuates rapidly, almost vanishing at the cascade, while the rotational
velocity profile produced by the actuator disc develops rapidly over the last
two thirds of the duct.

As before, Fig.16, hub and casing boundary layers were desirably
thin at inlet. The mainstream inlet velocity profile was represented
closely by

$$\frac{u_1'}{U_1} = -1 \cdot 928\theta + 0 \cdot 2792 .$$

Axial velocity profiles at Stations 1 to 5 are compared in Fig.26
with Theories A and B respectively.

Theory A predicted the outlet velocity at Station 4 to within 1%
over most of the duct. As mentioned above there was negligible difference
between Theories A and B at Station 4. At Stations 2, 3 and 5, however,
Theory B showed a great improvement over Theory A. Close agreement with
experiment was obtained at all stations. Slight secondary flow effects can
be observed at Stations 3 and 5 but these did not persist as far as Station 4.

The measured shear rates of the profiles are compared with the
predicted shear rate in Fig.25. This suggests that the position of the
actuator disc was well chosen at one third of the blade chord from the
leading edge. Fig.25 also shows that the theoretical rate of development
of the perturbations exceeded the experimental.

Fig.27 shows the swirling components of velocity at Stations 3,
5 and 4 compared with the assumption that (wR) remains constant along
conical surfaces. Agreement was excellent on this basis.

The total blade circulation Γ at a radius R is also equal to
the circulation around a circular path concentric with the axis and lying
on a cone.

$$\Gamma = 2\pi R w .$$

The constancy of circulation along the cone is also illustrated
in Fig.27, which shows the radial variation of circulation and gives some
idea of the streamwise vorticity shed from the cascade.

5.2 Non-uniform inlet stagnation pressure

The experiment was repeated with the conical gauze suspended in
the inlet contraction. The inlet velocity perturbation, Fig.28, consists
now of two components. The component, due to the inlet static pressure
variation, was approximately given by

$$\frac{u_1'}{U_1} = -0 \cdot 966\theta + 0 \cdot 1361$$

whereas that due to the smoke-ring vorticity was closely fitted by the curve

$$\frac{u_1''}{U_1} = -4 \cdot 0275\theta + 0 \cdot 5673 .$$

The points plotted in Fig.28 were computed from readings of p_o combined with the mean inlet static pressure.

The measured swirl angles, Fig.23a, compared well with those for irrotational inflow.

5.2.1 Theoretical prediction of axial velocity profile

There were three axial velocity perturbations to be considered.

The perturbation u' resulting from the variation of inlet static pressure may be treated as before by superimposing it upon the prediction obtained with the assumption of constant inlet static pressure

$$u' = u_1' \left(\frac{r}{r_1} \right)^{n-1} .$$

The velocity component u'' induced by the smoke-ring vorticity develops throughout the entire duct as before according to the law,

$$\frac{u''}{U} = \left(\frac{u_1''}{U_1} \right)\left(\frac{r}{r_1} \right)^4 .$$

Finally, we have to consider also the streamwise vorticity u''' shed from the cascade, which depends upon the sum of all three components at the cascade. From the evidence of the previous test, however, u' may be neglected at the cascade. The outlet velocity at Station 4, as derived in Appendix II, is then given by

$$\frac{u_2'}{U_2} = \left(\frac{r_2}{r_1} \right)^4 \left\{ 1 - 2 \left(\frac{r_m}{r_2} \right)^2 \right\} \frac{u_1''}{U_1}$$

$$+ \left(\frac{r_2}{r_m} \right)^2 \left\{ -1 + \frac{4 \frac{A}{a} \left(\frac{r_m}{r_1} \right)^4 \tan \alpha_m [2 + \frac{1}{3} \tan^2 \alpha_m] + K}{(2 + \tan^2 \alpha_m)^2} \right\}$$

$$\dots (19)$$

where

$$\frac{u_1''}{U_1} = A\theta + B$$

and

$$\tan \alpha_m = a\theta + b .$$

The axial velocity perturbations within the duct are

$$u' = u_1' \left(\frac{r}{r_1} \right)^{n-1} + u_1'' \left(\frac{r}{r_1} \right)^2 + \frac{1}{2} \left(\frac{r_m}{r} \right)^{n+2} u_2' \qquad \dots (20a)$$

upstream of the actuator disc, and

$$u' = u'_1 \left(\frac{r}{r_1} \right)^{n-1} + u''_1 \left(\frac{r}{r_1} \right)^2 + \left\{ 1 - \frac{1}{2} \left(\frac{r}{r_m} \right)^{n-1} \right\} u'_2 \qquad ...(20b)$$

downstream of tho actuator disc.

5.2.2 Comparison with experiment

The measured axial velocity components are compared with this analysis in Fig.29a. As before corrections were applied to the predictions at Stations 2, 3 and 5 to account for the variation of the unperturbed velocity across tho duct at those traversing stations. Excollent agreement was obtained throughout the duct. The profilo shear compares very well, confirming again that tho actuator disc was well positioned.

As in tho previous experimont tho axial velocity perturbations decroasod in magnitude botwoen Stations 1 and 2. Both the irrotational and the smoko-ring perturbations are attenuatod through tho contracting annulus. Approaching the blade row, howovor, tho actuator disc perturbations incroasod rapidly. In this case tho streamwiso vorticity was of the same design as tho smoke-ring vorticity, so that the profile shear rato incroasod in passing through the cascade to a valuo just loss than tho inlot shear rate. Tho shed stroamwiso vorticity was considerably strongor at outlot than tho smoko-ring vorticity.

The swirling velocity at Stations 3, 5 and 4 again comparod well with theory, Fig.29b.

6. Conclusions

A variety of experiments have boen described in which plane source and conical actuator disc theories have been investigated. These experiments have vorifiod interesting analytical conclusions about tho differing laws governing the rotational flows associated with two types of vorticity. These vorticity components, known as smoke-ring and stroamwiso vorticity, exist as a result of gradients, normal to the streamlinos, of stagnation pressure or angular momentum. The experiments have confirmed that in diverging flows these components must be considered separately. In cylindrical flow this necessity does not arise because vorticity flowing along the cylindrical flow surfaces remains constant in strength. In conical flow or any other type of diverging flow the vortex filaments are stretched sufficiently to change the two vorticities differentially. One incroases in magnitude while the other decreases.

The converging conical flow experiments have confirmed that the smoke-ring vorticity is attenuated by the contraction while the streamwiso vorticity is accentuated. The zero swirl experiment, Section 4.1, illustrated the attenuation of smoke-ring vorticity. The introduction of a streamwiso component similar in magnitude, but with only a small tangential component, caused little modification of the axial velocity profile which was still dominated by the smoke-ring vorticity and attenuated according to the law

$$\frac{u'_2}{U_2} = \lambda^2 \frac{u'_1}{U_1}$$

where λ is the ratio of outlet to inlet area.

Studies with free-vortex bladcs of large deflection illustratod that with irrotational inflow a conical free-vortex flow could be generated.

The/

The introduction of smoke-ring vorticity into the duct at inlet, however,
resulted in the shedding of streamwise vorticity from the blade row.
At outlet from the duct this streamwise vorticity increased in strength
to such an extent that its influence dominated that of the attenuated
smoke-ring vorticity.   In this case the two vorticities were of opposite
sign.   In consequence a reversal of shear rate of the profile occurred
between inlet and outlet.

Similar studies with a blade row producing a smaller swirl close
to solid rotation further illustrated these effects.   With irrotational
inflow streamwise vorticity was generated at the blade row.   The
introduction of smoke-ring vorticity gave rise to a slight modification
of the streamwise vorticity appearing at the cascade.   In this case the
vorticities were of the same sign so that reversal of the profile shear
rate did not occur.   Equally good agreement with theory was obtained.

7.   Acknowledgments

This work was conducted at the Cambridge University Engineering
Laboratory.   The author is now employed with the English Electric Company Ltd.,
Mechanical Engineering Laboratory, Whetstone.

References

No.	Author(s)	Title, etc.
1	H. Cohen and E. M. White	The theoretical determination of the three-dimensional flow in an axial compressor with special reference to constant reaction blading. A.R.C.6 842, 1943.
2	W. R. Hawthorne and J. H. Horlock	Actuator disc theory of the incompressible flow in axial compressors. Proc.I.Mech.E., Vol.176, No.30, 1962.
3	F. E. Marble	The flow of a perfect fluid through an axial turbo-machine with prescribed blade loading. Journ. Aero. Sci., Vol.15, 1948.
4	S. L. Bragg and W. R. Hawthorne	Some exact solutions of the flow through annular cascade actuator discs. Journ. Aero. Sci., Vol.17, p.243, 1950.
5	J. H. Horlock	Some actuator-disc theories for the flow of air through an axial turbo-machine. A.R.C. R. & M. No.3030, December, 1952.
6	A. D. Carmichael and J. H. Horlock	Actuator disc theories applied to the design of axial compressors. A.R.C. Current Paper No.315, April, 1956.
7	J. F. Louis and J. H. Horlock	A graphical method of predicting the off-design performance of a compressor stage. A.R.C. Current Paper No.320, April, 1956.
8	J. H. Horlock	Experimental and theoretical investigations of the flow of air through two single-stage compressors. A.R.C. R. & M. No.3031, March, 1955.

No.	Author(s)	Title, etc.
9	J. H. Horlock and E. C. Deverson	An experiment to determine the position of an equivalent actuator disc replacing a blade row of a turbo-machine. A.R.C. Current Paper No.426, March, 1958.
10	D. S. Whitehead and G. S. Beavers	A single-parameter theory of vortex flow in turbo-machines. A.R.C. R. & M. No.3335. August, 1961.
11	J. H. Horlock and R. I. Lewis	Shear flows in straight sided nozzles and diffusers. Int. J. Mech. Sci., Vol.2, p.251. 1961.
12	R. I. Lewis and J. H. Horlock	Non-uniform three-dimensional and swirling flows through diverging ducts and turbo-machines. Int. J. Mech. Sci., Vol.3, p.170. 1961.
13	R. I. Lewis	A theoretical investigation of the rotational flow of incompressible fluids through axial turbo-machines with tapered annulus walls. Int. J. Mech. Sci., Vol.6, pp.55-75. 1963.
14	R. I. Lewis	Flow through non-cylindrical axial turbo-machines. Cambridge University Thesis, 1960.
15	R. I. Lewis	Annular cascade wind tunnel. The Engineer, Vol.215, 1963, pp.341-344.
16	D. G. Ainley and G. C. R. Lathieson	A method of performance estimation for axial-flow turbines. A.R.C. R. & M.2974, December, 1951.
17	F. A. L. Winternitz	Cantilevered pitot cylinder. The Engineer, Vol.199, p.729, 1955.

- 20 -

APPENDIX I

Notation

Z, R, θ cylindrical co-ordinates

ψ Stokes' stream function

$u = -\dfrac{1}{R}\dfrac{\partial\psi}{\partial R}$ velocity in Z direction

$v = \dfrac{1}{R}\dfrac{\partial\psi}{\partial Z}$ velocity in R direction

w velocity in θ direction

q velocity vector

ρ fluid density

p static pressure

$p_0 = p + \tfrac{1}{2}\rho\, q^2$ stagnation pressure

$$\eta = \frac{\partial v}{\partial Z} - \frac{\partial u}{\partial R}$$

     vorticity in θ direction

$$= (w)\frac{d(wR)}{d\psi} - \frac{R}{\rho}\frac{dp_0}{d\psi}$$

r, θ, ϕ spherical co-ordinates

u velocity in r direction

v velocity in θ direction

w velocity in ϕ direction

$U = \dfrac{C}{r^2}$ irrotational source velocity $(C = \text{constant})$

$w = \dfrac{K}{R}$ free vortex swirl velocity $(K = \text{constant})$

λ ratio of outlet to inlet area of diffuser or contraction

u', v' rotational velocity perturbations

u' perturbation due to static pressure gradient

u'' perturbation due to smoke-ring vorticity

u''' perturbation due to streamwise vorticity

APPENDIX II

Application of Conical Actuator Disc Theory
to Flow through Blade Rows

Equations are derived in this Appendix for flow through free
vortex and near solid rotation blade rows situated in a conical annulus.

The theoretical model is shown in Fig.1. Inlet and outlet
planes are represented by spherical surfaces r_1 and r_2 at which the
fluid is assumed to be in radial equilibrium, Ref.12.

Radial Equilibrium

The condition of radial equilibrium or cylindrical flow can be
expressed in spherical co-ordinates as follows:

$$\frac{1}{\rho}\frac{\partial p_o}{\partial \theta} = \frac{w}{\sin \theta}\frac{\partial}{\partial \theta}(w \sin \theta) + u \frac{\partial u}{\partial \theta} . \qquad \ldots (2.1)$$

If p_o is assumed to be a function of θ only we have

$$\frac{\partial p_{o1}}{\partial \theta} = \frac{\partial p_{o2}}{\partial \theta}$$

where suffices $_1$ and $_2$ refer to Stations 1 and 2. Suffix m will
refer to the actuator disc.

If second order products of the perturbations are neglected
equation (2.1) yields

$$\frac{\partial u'_2}{\partial \theta} = \left(\frac{r_2}{r_1}\right)\frac{\partial u'_1}{\partial \theta} - \frac{w_2}{U_2 \sin \theta}\frac{\partial}{\partial \theta}(w_2 \sin \theta) . \qquad \ldots (2.2)$$

Conical Actuator Disc Solution

The conical actuator disc solution, Ref.12, for the axial
velocity perturbation within the duct is as follows:

$$u' = \left\{ \frac{u''_1}{r_1^2} + \frac{1}{2}\left(\frac{u''_2}{r_2^2} - \frac{u''_1}{r_1^2}\right)\left(\frac{r}{r_m}\right)^{n-1} \right\} r^2$$

upstream of r_m $\ldots (2.3a)$

$$+ \left\{ u'''_1 + \tfrac{1}{2}(u'''_2 - u'''_1)\left(\frac{r}{r_m}\right)^{n-1} \right\}$$

$u'/$

$$u' = \left\{ \frac{u''_2}{r_2^2} - \frac{1}{2} \left(\frac{u''_2}{r_2^2} - \frac{u''_1}{r_1^2} \right) \left(\frac{r}{r_m} \right)^{-n-2} \right\} r^2$$

$$\text{downstream of } r_m \quad ...(2.3b)$$

$$+ \left\{ u'''_2 - \tfrac{1}{2}(u'''_2 - u'''_1) \left(\frac{r}{r_m} \right)^{-n-2} \right\} .$$

In the plane of the actuator disc we have

$$u'_m = \frac{1}{2} \left(\frac{u''_1}{r_1^2} + \frac{u''_2}{r_2^2} \right) r_m^2 + \tfrac{1}{2}(u'''_1 + u'''_2) . \qquad ... (2.4)$$

Double and treble primes refer to the contributions of smoke-ring and streamwise vorticity components respectively.

Another result given in Ref.12 is

$$wr \sin \theta = f(\theta) . \qquad ... (2.5)$$

General Equation for Conical Duct containing Actuator Disc

If there is zero swirl upstream of r_m

$$u'''_1 = 0$$

and if there is no change in p_0 at the actuator disc

$$\frac{u''_1}{r_1^2} = \frac{u''_m}{r_m^2} = \frac{u''_2}{r_2^2}$$

this follows from equation (9).

Equation (2.4) then becomes

$$\frac{\partial u'_2}{\partial \theta} = 2 \frac{\partial u'_m}{\partial \theta} - \left(\frac{r_2}{r_1} \right)^2 \left\{ 2 \left(\frac{r_m}{r_2} \right)^2 - 1 \right\} \frac{\partial u'_1}{\partial \theta} . \qquad ... (2.6)$$

Also equation (2.5) yields

$$w_2 = \left(\frac{r_m}{r_2} \right) (U_m + u'_m) \tan \alpha \qquad ... (2.7)$$

where α is the outlet angle from the actuator disc.

Equations (2.6) and (2.7) may be introduced into the radial equilibrium equation (2.2). If second order products of perturbations are again neglected the following first order differential equation for u'_m is obtained.

$$\frac{d}{d\theta}\left(\frac{1}{2} + \frac{u'_m}{U_m}\right) + F_1\left(\frac{1}{2} + \frac{u'_m}{U_m}\right) = F_2\frac{d}{d\theta}\left(\frac{u'_1}{U_1}\right) \qquad \dots (2.8)$$

where

$$F_1 = \frac{2\cot\theta\,\tan^2\alpha + \frac{d}{d\theta}(\tan^2\alpha)}{2 + \tan^2\alpha} \qquad \dots (2.9)$$

and

$$F_2 = \frac{\left(\dfrac{r_m}{r_1}\right)^4}{2 + \tan^2\alpha}. \qquad \dots (2.10)$$

Solutions of equation (2.8), which is general, can be found for cascade outlet angles which are simple functions of θ. The general solution is as follows:

$$\frac{u'_m}{U_m} = -\frac{1}{2} + \left(\frac{r_m}{r_1}\right)\frac{\displaystyle\int F_3 F_2\frac{d}{d\theta}\left(\frac{u'_1}{U_1}\right)d\theta}{F_3} \qquad \dots (2.11)$$

where

$$F_3 = (e)^{\int F_1\,d\theta}. \qquad \dots (2.13)$$

Solution for Free Vortex Cascade

The cascade outlet angle distribution required for the generation of a free vortex conical swirl is

$$\tan\alpha = \frac{\tan\alpha_1\,\sin\theta}{\sin\theta_1}$$

suffix $_1$ referring to the hub.

With constant static pressure at inlet and a velocity variation given by

$$\frac{u''_1}{U_1} = a\sin\theta + b$$

the solution for the outlet velocity, using equation (2.11) is

$$\frac{u'_2}{U_2}$$

- 24 -

$$\frac{u'_2}{U_2} = \left(\frac{r_2}{r_1}\right)^4 \left\{ \sin\theta - \sqrt{2}\tan\alpha_1 \sin\theta_1 \left(\frac{r_m}{r_2}\right)^2 \right.$$

$$\left. - \tan^{-1}\left[\frac{\sqrt{2}\sin\theta}{\tan\alpha_1 \sin\theta_1}\right] \right\} a + c \qquad \dots (2.14)$$

where c is chosen graphically such that

$$\int_{\theta_1}^{\theta_2} \frac{u'_2}{U_2} \sin\theta \, d\theta = 0 \qquad \dots (2.15)$$

which satisfies the condition of continuity of mass flow through the annulus.

Solution for Near Solid Rotation Cascade

If $\qquad \tan\alpha = a\theta + b$

and θ is small, equation (2.9) approximates to

$$F_1 = \frac{\dfrac{2}{\theta}\tan^2\alpha + \dfrac{d}{d\theta}(\tan^2\alpha)}{2 + \tan^2\alpha} .$$

With constant inlet static pressure and a velocity distribution given by

$$\frac{u'_1}{U_1} = A\theta + B .$$

The outlet velocity, by equation (2.11) becomes

$$\frac{u'_2}{U_2} = \left(\frac{r_2}{r_1}\right)^4 \left\{ 1 + 2\left(\frac{r_m}{r_2}\right)^2 \right\} \frac{u'_1}{U_1} - \left(\frac{r'_2}{r_m}\right)^2$$

$$+ \frac{4\dfrac{A}{a}\left(\dfrac{r_2}{r_1}\right)^2\left(\dfrac{r_m}{r_1}\right)^2 \tan\alpha\left(2 + \tfrac{1}{3}\tan^2\alpha\right) + K_1}{(2 + \tan^2\alpha)^2}$$

where K_1 is a constant determined by equation (2.15).

If, on the other hand the inlet velocity perturbation is an irrotational one, and the stagnation pressure is constant, equations (2.3) and (2.4) have an additional term u''''

$u''''/$

- 25 -

$$u'''' = u_1' \left(\frac{r}{r_1} \right)^{n-1}$$

both upstream and downstream of the actuator disc. In other words, the inlet pressure or velocity perturbation decays progressively through the duct. At the cascade the velocity perturbation is

$$u_m' = K \cdot \tfrac{1}{2}u_2'$$

where

$$K = 1 + 2 \frac{u_1'}{u_2'} \left(\frac{r_1}{r_m} \right)^{n-1} .$$

If this result is introduced into equation (2.2) one has finally

$$\frac{u_2'}{U_2} = \frac{1}{K} \left(\frac{r_2}{r_m} \right)^2 \left\{ \frac{K_3}{\left(\frac{2}{K} + \tan^2\alpha \right)^2} \right\} - 1 . \qquad \ldots (2.16)$$

APPENDIX III /

APPENDIX III

Corrections to Probe Readings

1. Correction for the Angle of Inclination of a Probe to the Flow

The relation of the probe to the velocity vector q in conical flow is shown in Fig.30. The velocity may be resolved in two ways. It may be regarded as the vector sum of axial and tangential components u and w. Alternatively q may be resolved into a component q_1 normal to the probe and a component q_2 parallel with the probe axis. If the probe were infinitely thin the readings would be unaffected by q_2 and the dynamic head registered would be

$$\tfrac{1}{2}\rho q_1^2 \;=\; \tfrac{1}{2}\rho q^2 \cos^2\beta \;.$$

Measurements made by Winternitz[17] with a cylindrical pitot probe showed a fair measure of agreement with the cosine squared law. Applying this result to conical flow with a swirl angle α, the measured and actual velocities are related as follows:

$$q_1^2 \;=\; q^2\,(1 - \cos^2\alpha\,\sin^2\theta)$$

and also
$$\frac{\text{True dynamic head}}{\text{Recorded dynamic head}} \;=\; \frac{1}{1 - \cos^2\alpha\,\sin^2\theta} \;.$$

The recorded swirl angle α' is related to the actual swirl angle on a conical surface by

$$\frac{\tan\alpha}{\tan\alpha'} \;=\; \sec\theta \;.$$

2. Variation of the Irrotational Source Velocity at a Plane Traversing Station

In the conical duct experiments traversing stations were plane rather than spherical surfaces. The theoretical predictions were based on the model shown in Fig.1. At Station m within the duct the irrotational velocity U varies from hub to casing because of the variation of r the radial distance from the point source to the traversing plane. If this distance is equal to r_m at the centre of the annulus θ_m, then

$$r_m \cos\theta_m \;=\; r\cos\theta$$

and
$$U \;=\; U_m \left(\frac{\cos\theta}{\cos\theta_m} \right)^2 \;.$$

If θ and θ_m are expanded as a series, then for small values of θ we have approximately

$$\frac{U}{U_m} = 1 + \theta_m^2 - \theta^2 .$$

For the duct used in the experiments this ratio is as follows:

| $\dfrac{\theta - \theta_1}{\theta_2 - \theta_1}$	$\dfrac{U}{U_m}$
0	1·01492
0·2	1·00918
0·4	1·00496
0·6	1·00000
0·8	0·99436
1·0	0·98307

DR

FIG. 1

CYLINDRICAL POLAR COORDINATE SYSTEM
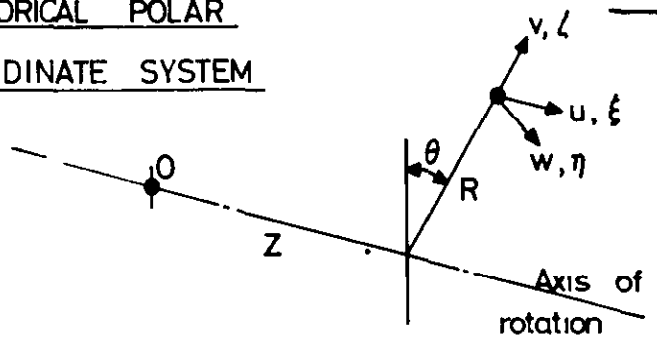
Actuator disc
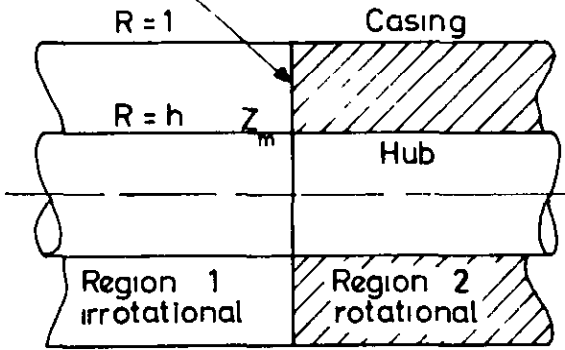
MODEL FOR CYLINDRICAL ACTUATOR DISC THEORY

Region 1 irrotational

Region 2 rotational

SPHERICAL COORDINATE SYSTEM
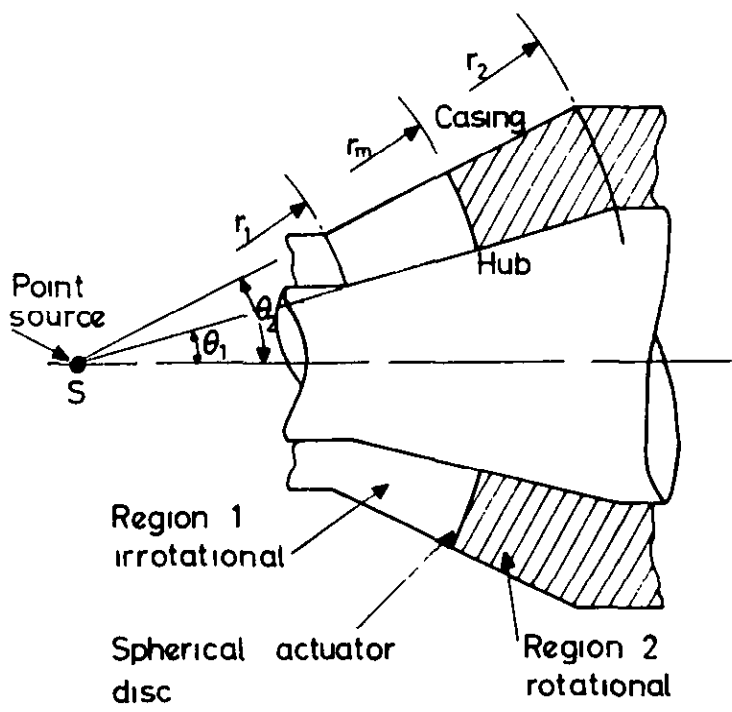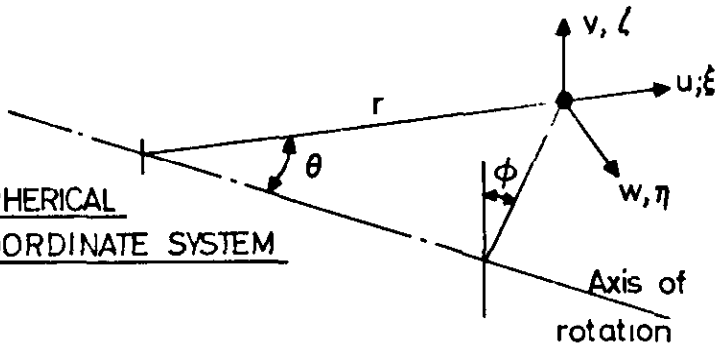
MODEL FOR CONICAL ACTUATOR DISC THEORY

Point source

Region 1 irrotational

Spherical actuator disc

Region 2 rotational

u, v, w   Velocity components

ξ, ζ, η Vorticity components

CYLINDRICAL AND SPHERICAL COORDINATE SYSTEMS

AND MODELS FOR

CYLINDRICAL AND CONICAL ACTUATOR DISC THEORIES.

FIG. 2

Streamwise vorticity

Smoke-ring vorticity

Velocity and vorticity components

q, Ω

η

v, ζ

w, η

u, ξ

R

Z

Axis of rotation
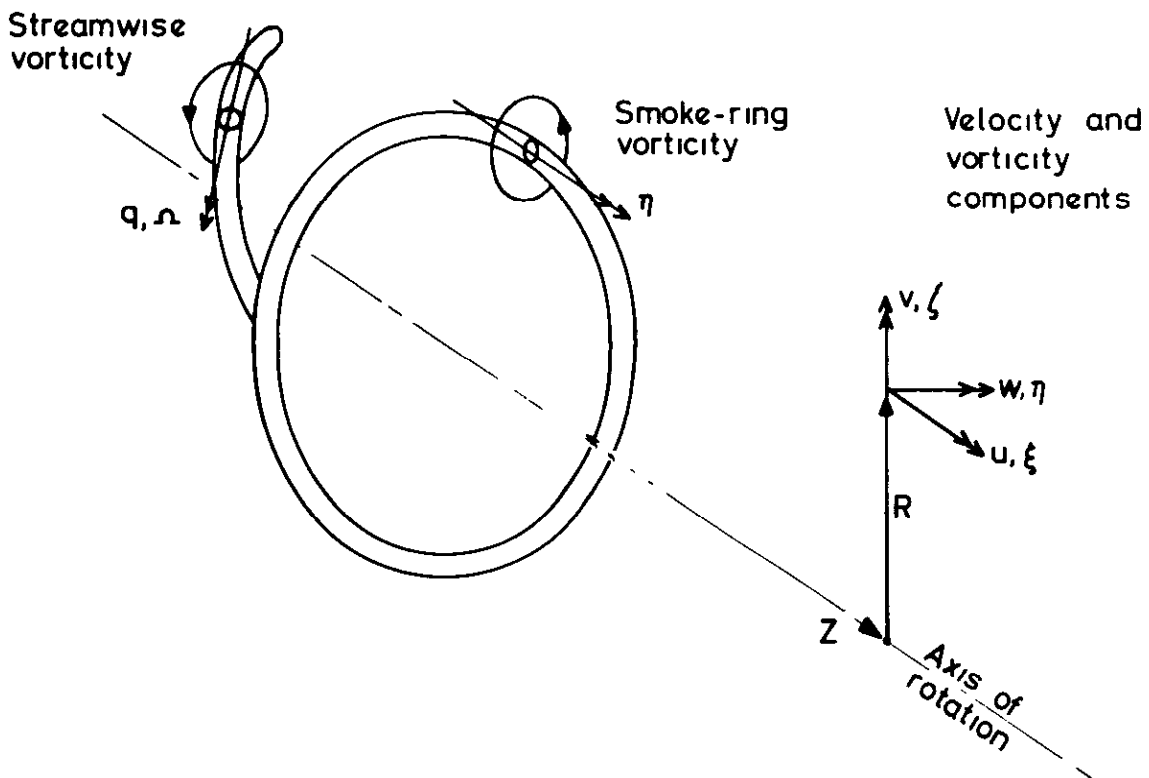
SHOWING ELEMENTARY VORTEX TUBES OF
STREAMWISE AND SMOKE-RING VORTICITY.

PLAN VIEW OF DUCT

Gauze No 1

Gauze No 2
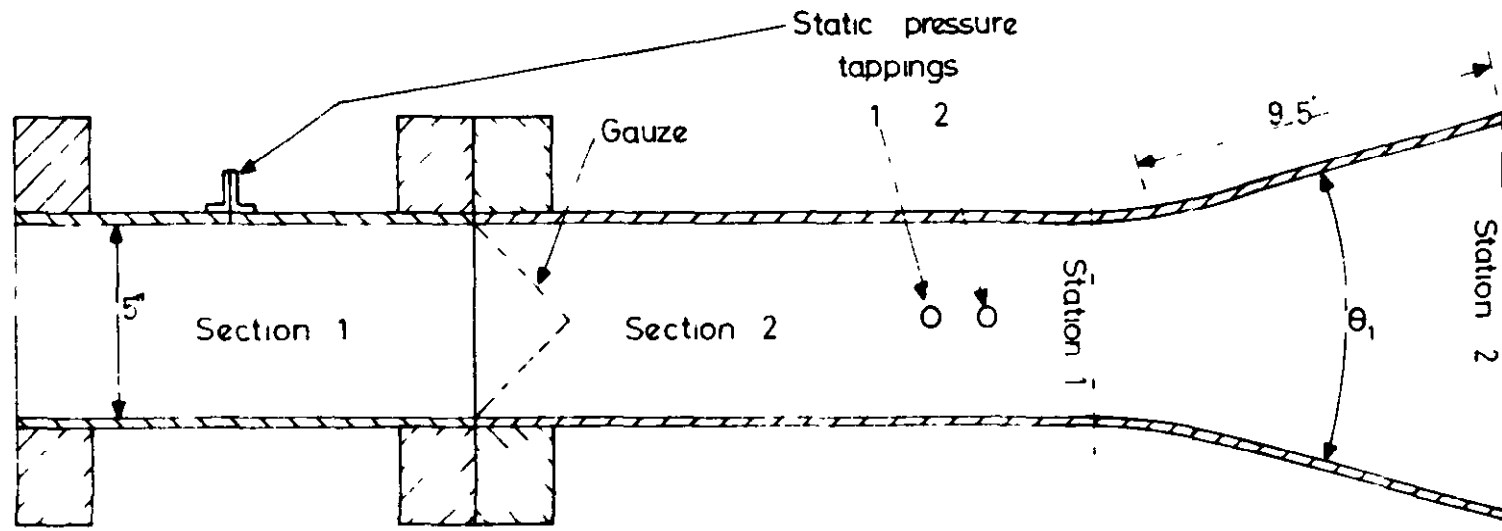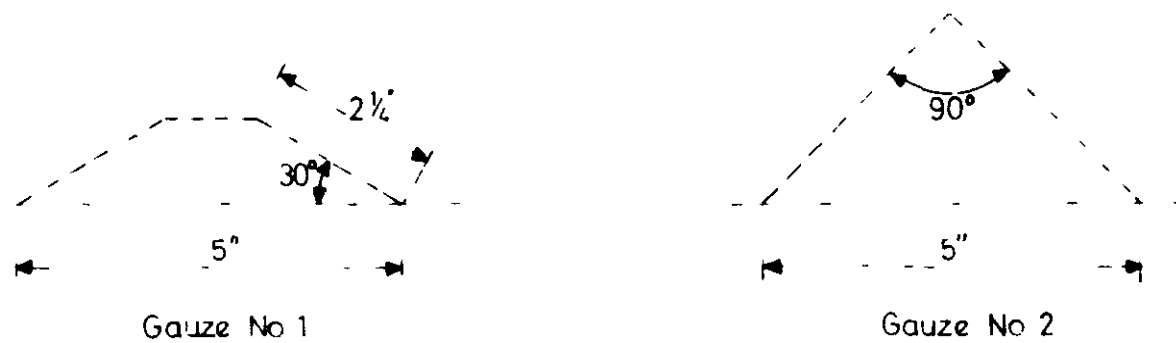
FIG.3
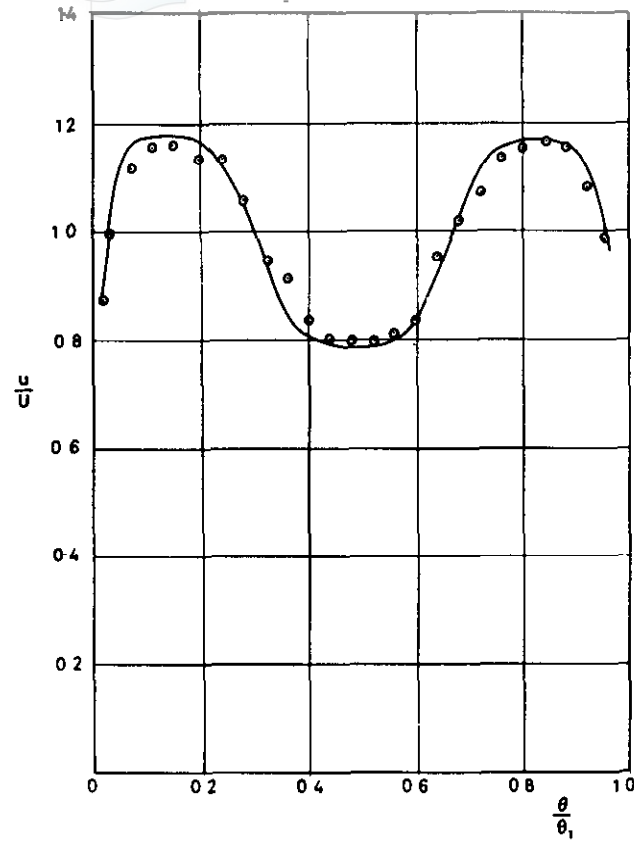
FIG 4

U = 73.3 ft/sec.

λ = 1.0   Full curve   Station 1

θ = 0°   •   Station 2

FIG 4 (a) VELOCITY PROFILES AT STATIONS 1 & 2

WITH PARALLEL SIDE WALLS SHOWING NEGLIGIBLE

ATTENUATION OF STRONGLY SHEARED FLOW
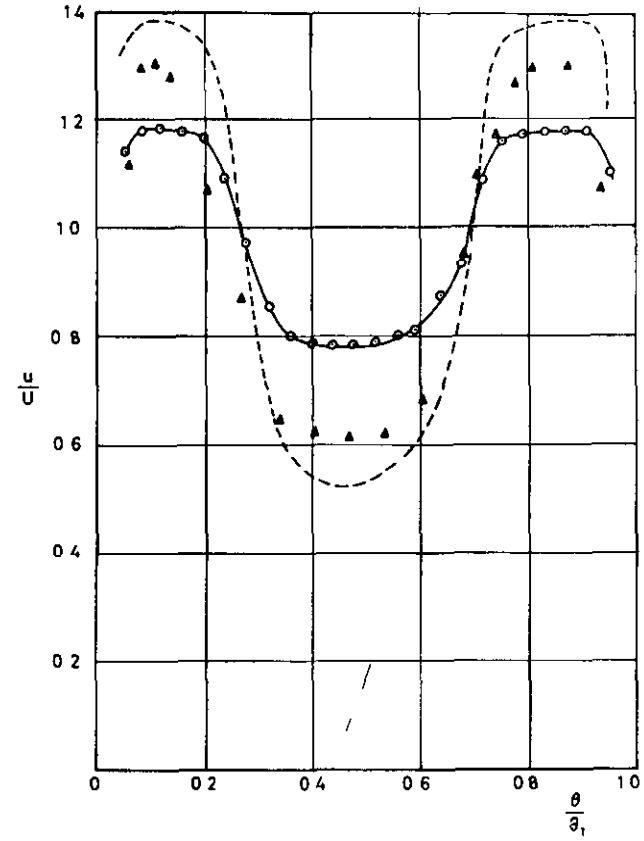
λ = 1.47   ○ Station 1 } Experimental

θ = 15°   ▲ Station 2 }   points

Dashed curve shows predicted velocity profile at Station 2

FIG 4 (b) COMPARISON OF EXPERIMENTAL AND PREDICTED

VELOCITY PROFILES FOR FLOW THROUGH 15° DIFFUSER

VELOCITY PROFILES FOR FLOW		Date	March 1963
THROUGH PARALLEL AND		Drawing No	R20172 - 3185
DIVERGING TWO-DIMENSIONAL DUCTS		Report No	W/M(2A) p 74
		Figure Sheet No	4

FIG. 5
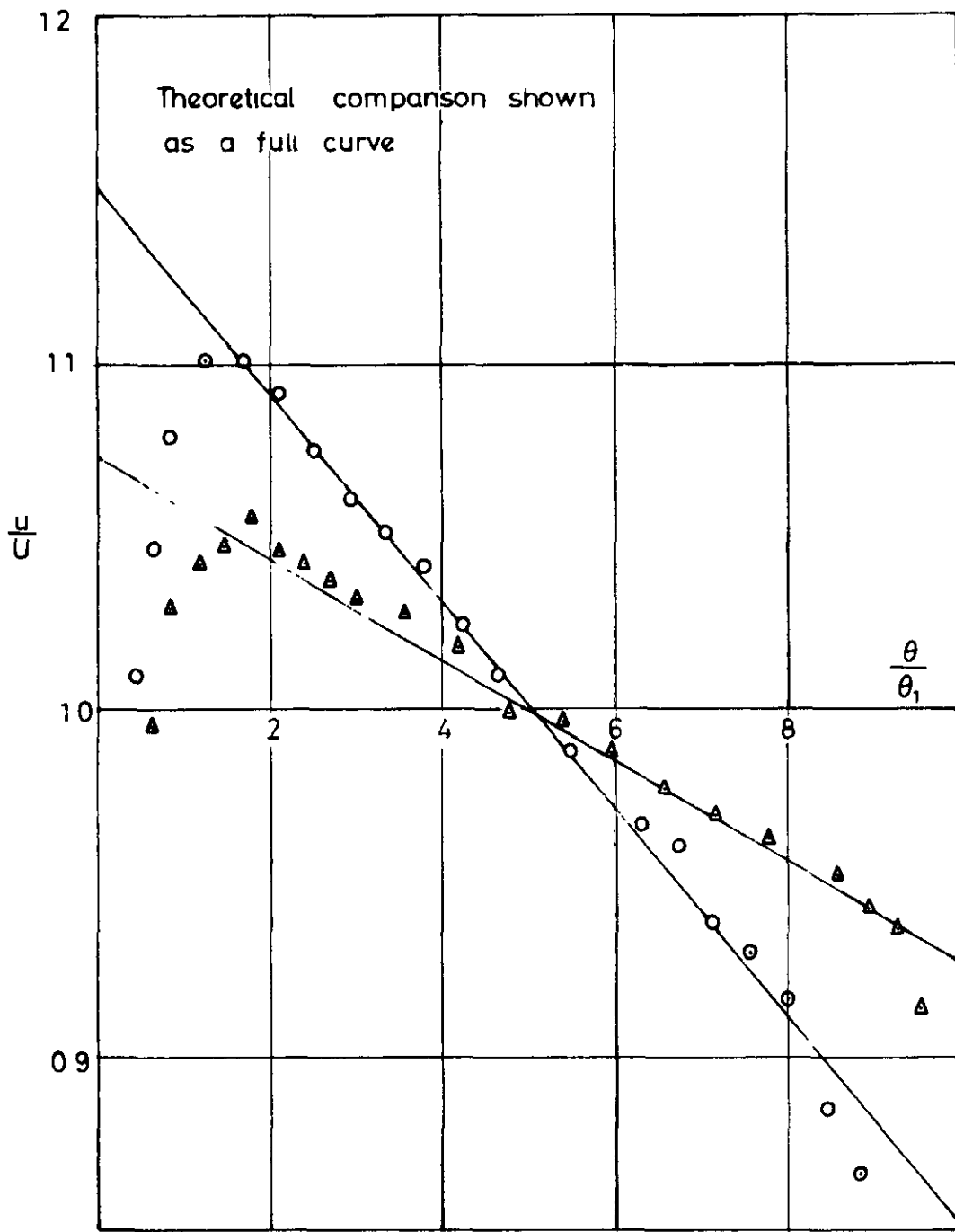
ATTENUATION OF A LINEAR SHEAR PROFILE THROUGH A TWO-DIMENSIONAL 10° CONTRACTION.
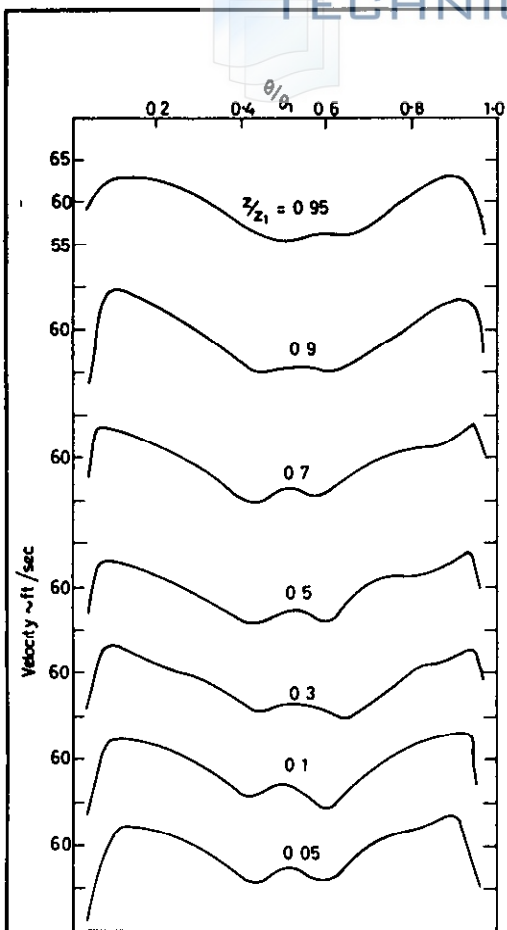
FIG 6

FIG 6(a) VELOCITY PROFILES AT STATION 1
WITH GAUZE No 1
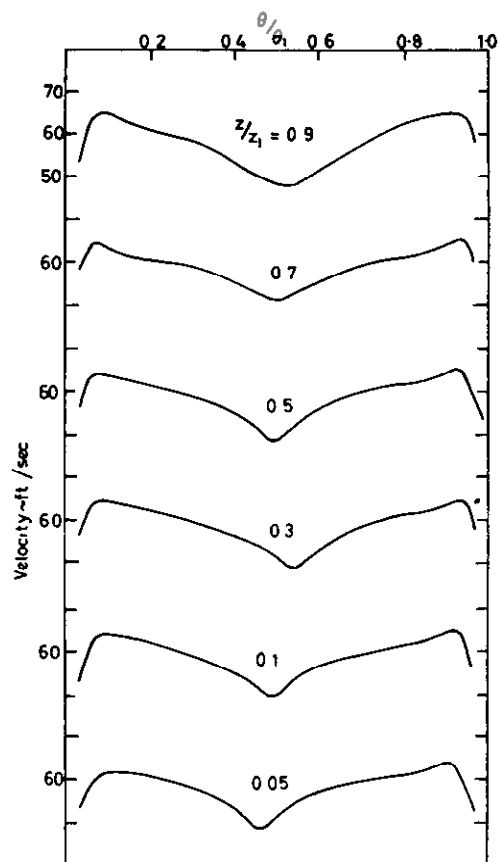
FIG 6(b) VELOCITY PROFILES AT STATION 1
WITH GAUZE No 2
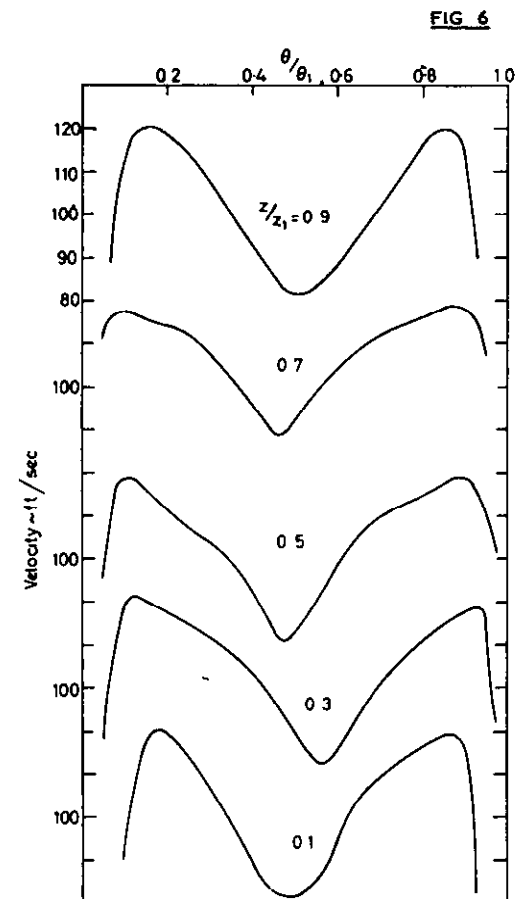
FIG 6(c) OUTLET VELOCITY AT STATION 2 WITH
GAUZE No 2 & 12.1° OF DIVERGENCE

z/z_1 = Height of traversing plane relative to bottom of duct

VELOCITY TRAVERSES TAKEN AT
STATIONS 1 & 2 OF DIVERGING DUCT
TO CHECK ON TWO-DIMENSIONAL
NATURE OF FLOW

Dashed curve shows theoretical outlet velocity and

full curve inlet velocity

Experiment shown thus – o

CHANGE IN VELOCITY PROFILE THROUGH A 10°

DIFFUSER AND A 10° CONTRACTION ~ GAUZE No.1
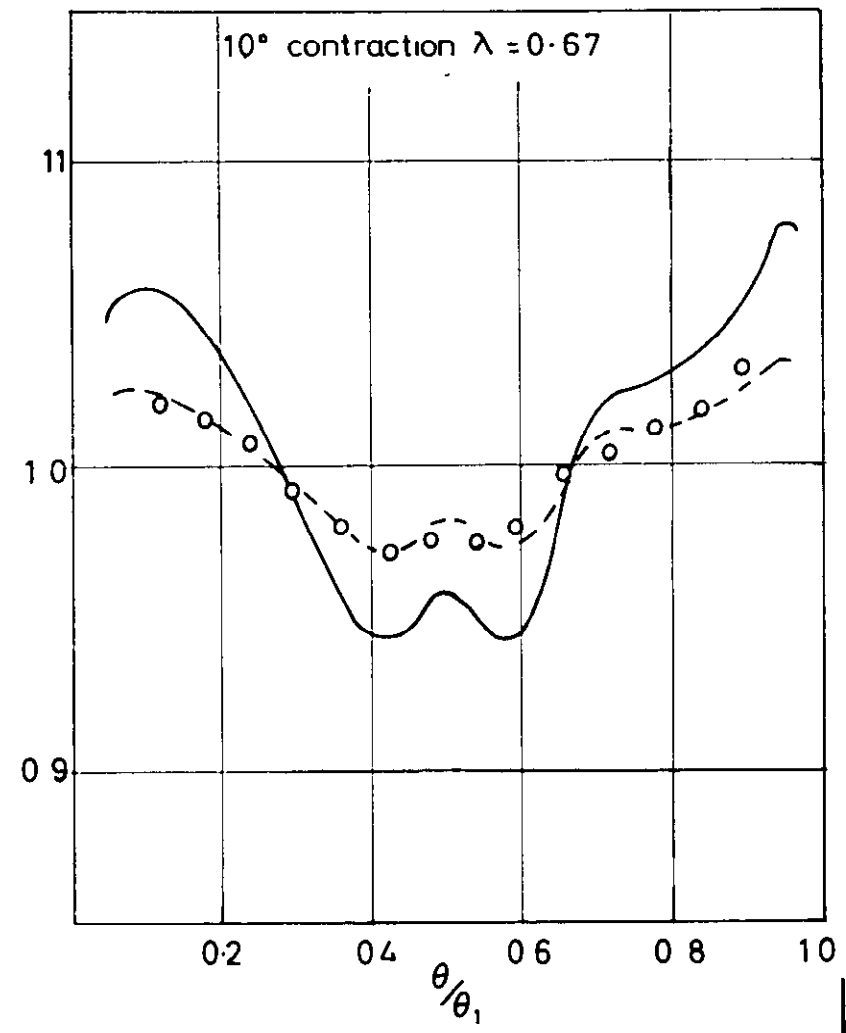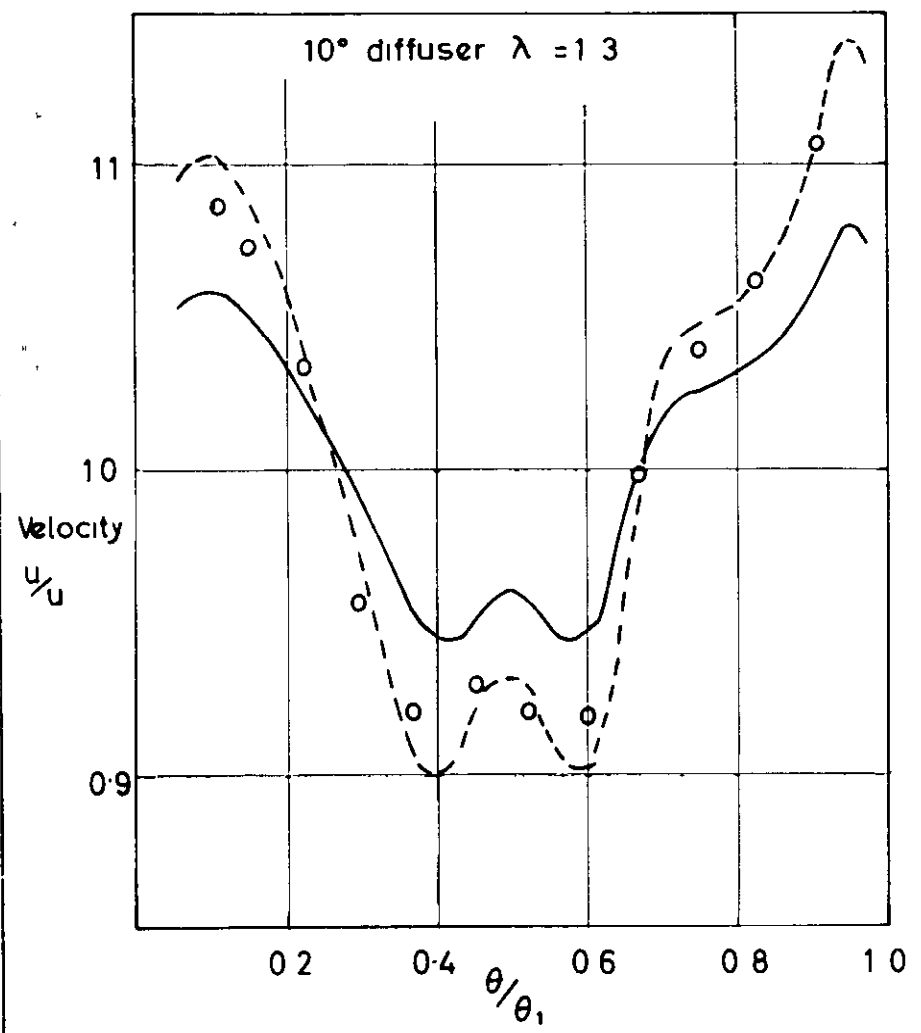
FIG. 7

FIG. 8

Full curve ~ inlet profile

Dotted curve ~ theoretical outlet profile

o ~ Experimental outlet profile

$\theta_1 = 12\ 1°$

Area ratio $\lambda = 1\ 4$
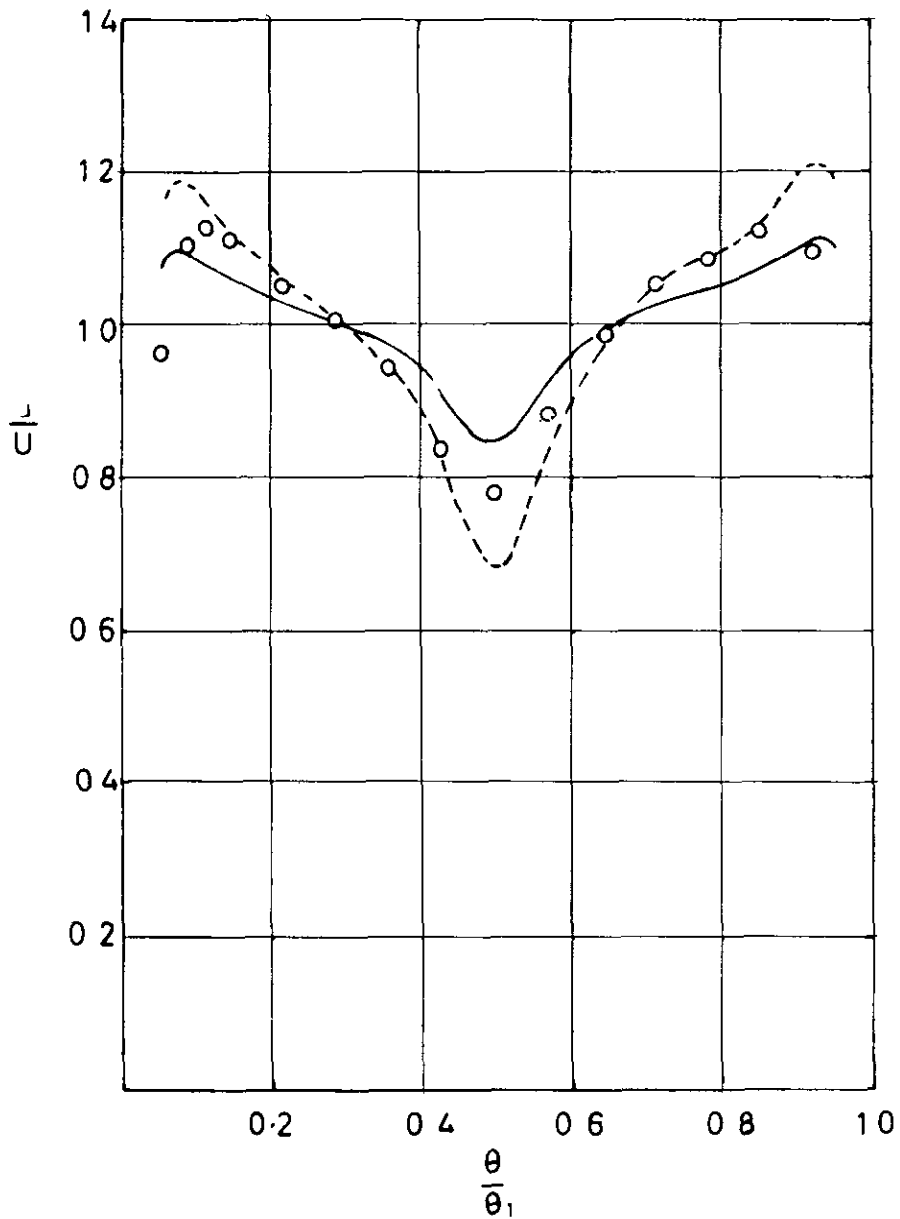
CHANGE IN VELOCITY PROFILE THROUGH

A 12·1° TWO DIMENSIONAL DIFFUSER ~

GAUGE No. 2

FIG. 9
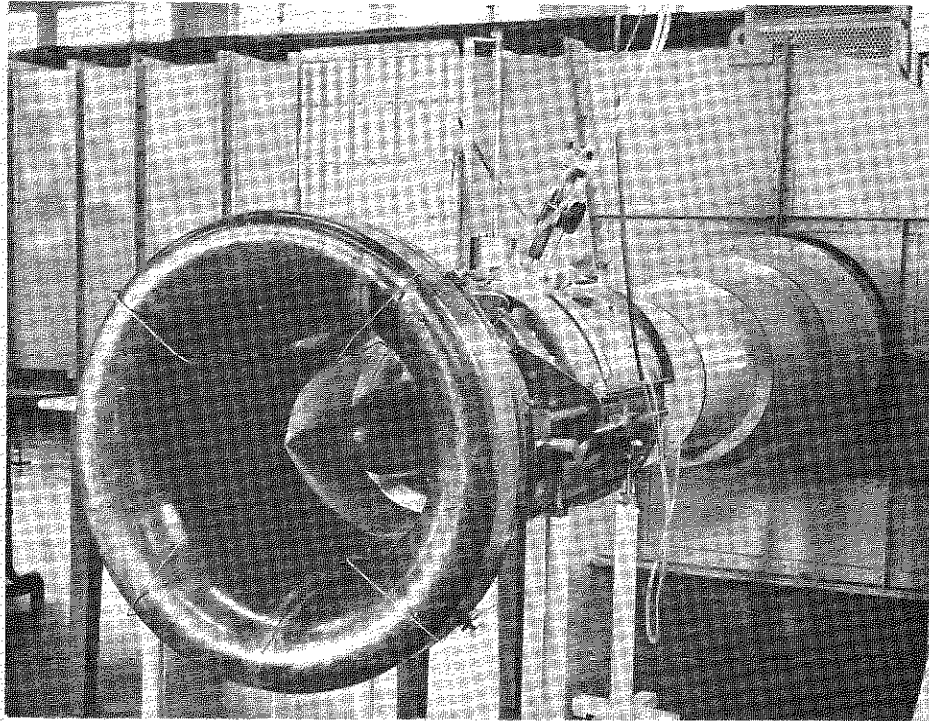
FIG. 9 (a)   ANNULAR   CASCADE   WIND   TUNNEL
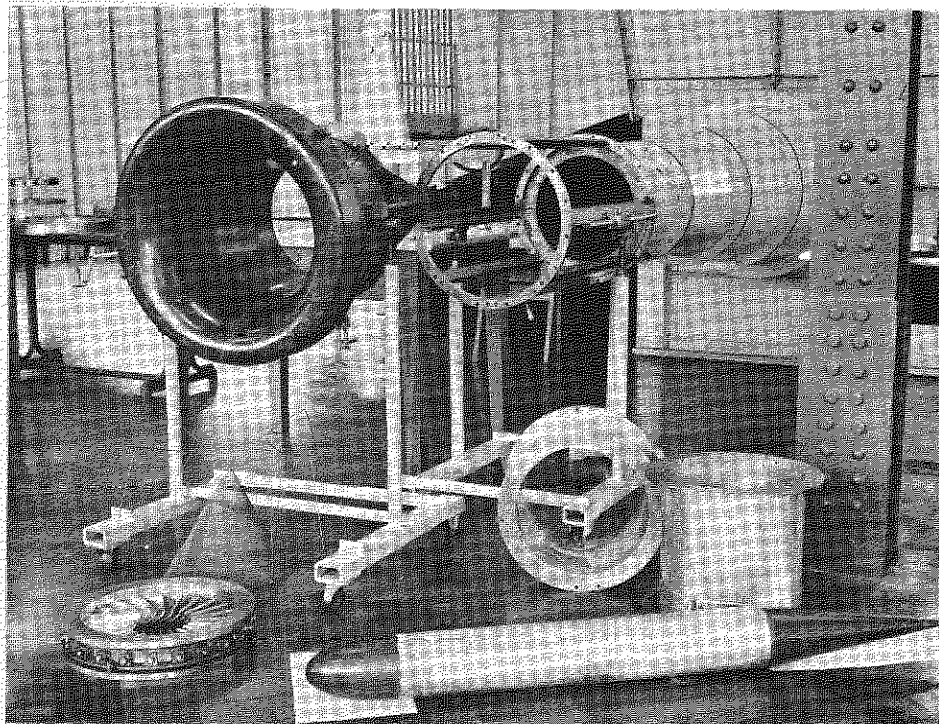
FIG. 9 (b)   COMPONENTS   OF   ANNULAR   CASCADE
WIND   TUNNEL.

VIEWS OF ANNULAR CASCADE WIND TUNNEL.

FIG 10

Positions for
traversing probes

Inlet gauze

Hub

Diffuser

Conical
section

S

Cylindrical
section 'B

Inlet contraction

Working section

Outlet section

1 r_1 2 3 5 r_2 4

Converging duct

1 r_1 2   3 r_2 4

A   B   C   D

Diverging duct

TRAVERSING STATIONS,

| | | ANNULAR CASCADE CONICAL DUCT | |
| | | ASSEMBLY AND TRAVERSING STATIONS | |
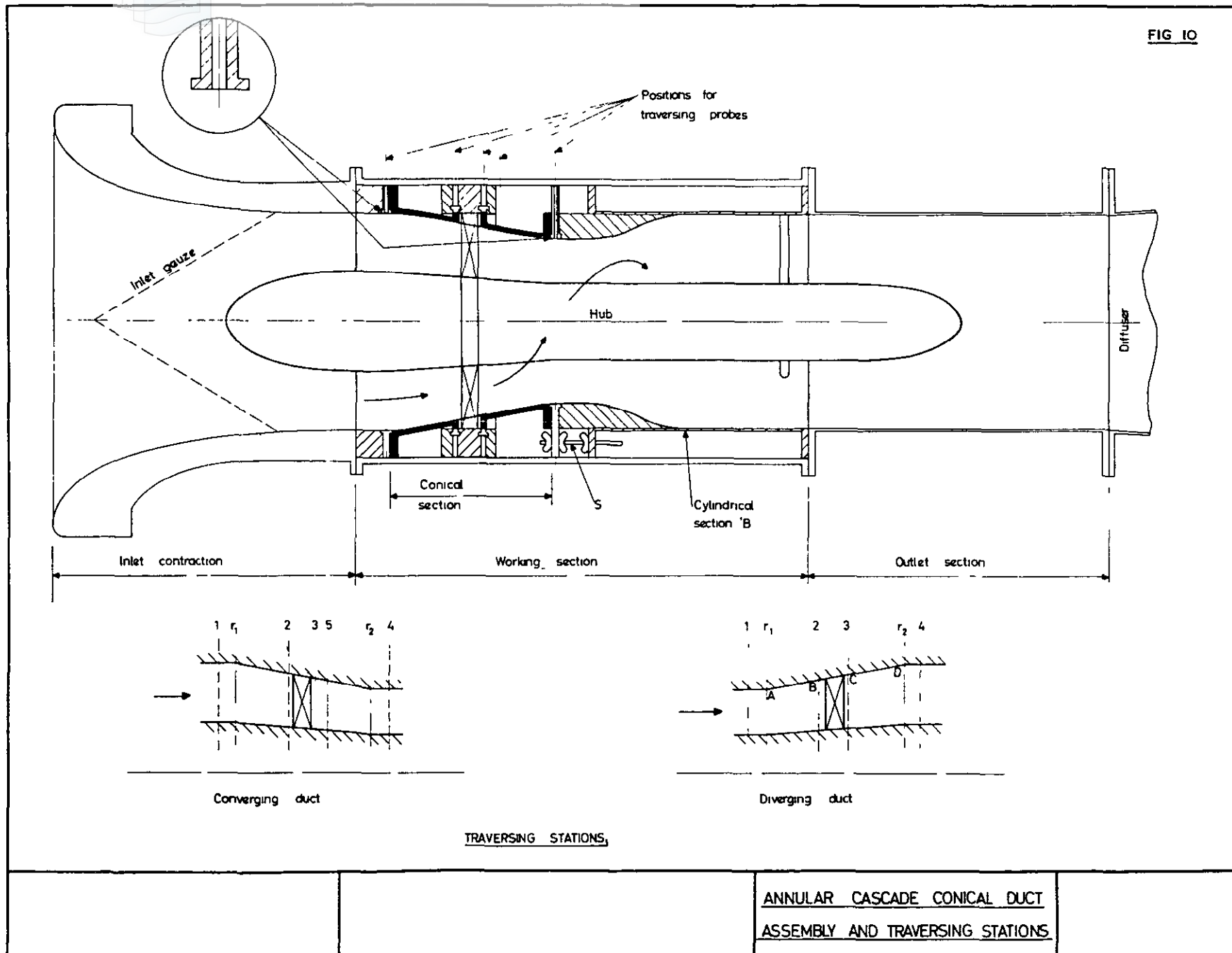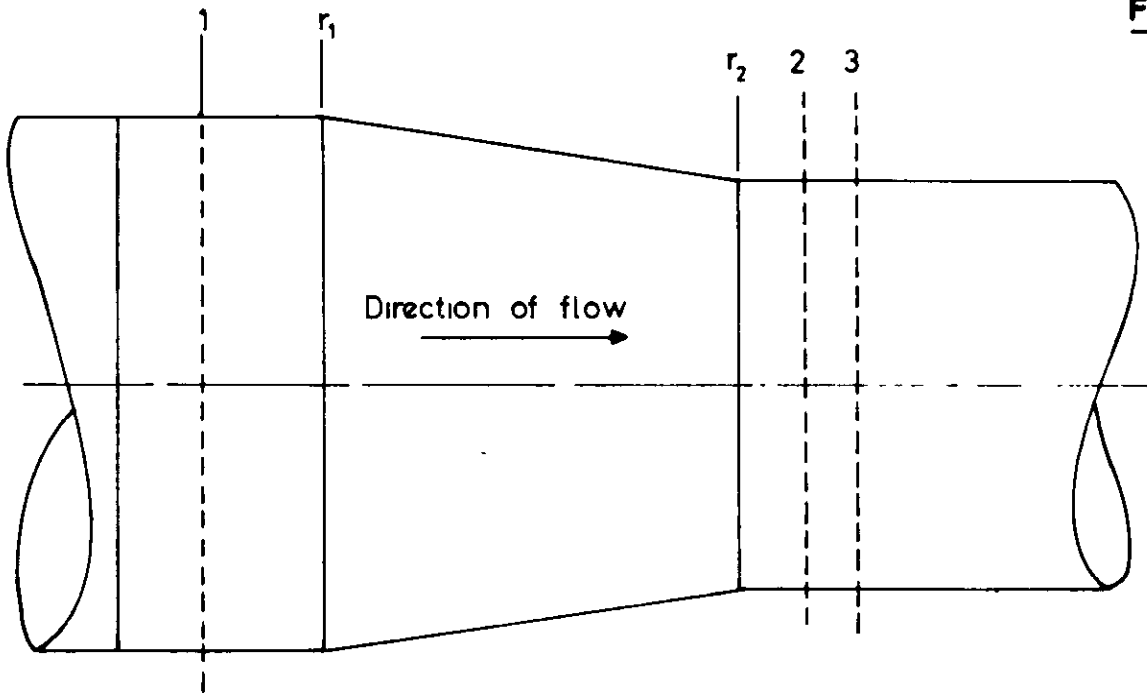
FIG. 11

FIG 11(a) DUCT FOR NON-SWIRLING FLOW

Direction of flow

Inlet guide vanes
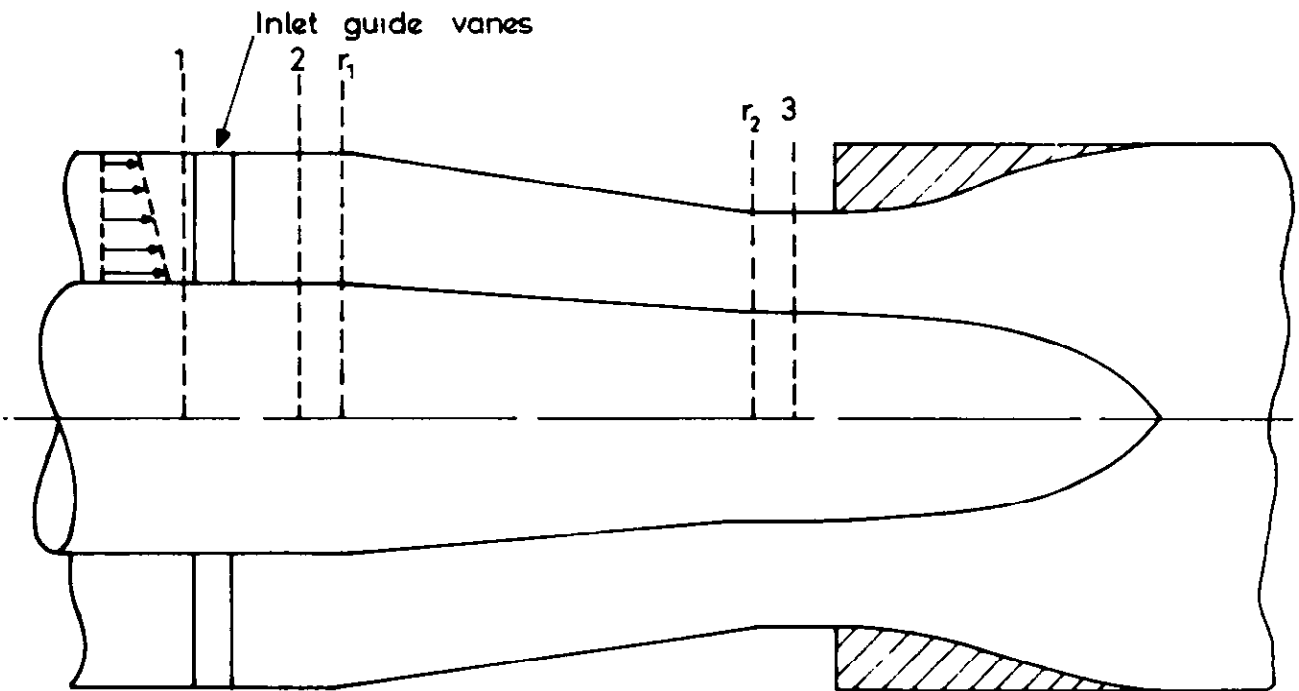
FIG. 11 (b) DUCT WITH SMALL AMOUNT OF SWIRL.

CONICAL DUCTS FOR NON SWIRLING & SMALL SWIRLING

EXPERIMENTS.

FIG 12

Station 1

Station 2

Station 3

Probe position $\frac{\theta}{\theta_1}$

Static depression = (Atmospheric pressure − measured pressure)
Inches of maths

STATIC PRESSURE TRAVERSES
AT STATIONS 1, 2 & 3

Station 2

Station 1

Velocity ft/sec

Probe position $\frac{\theta}{\theta_1}$

VELOCITY TRAVERSES AT
STATIONS 1&2
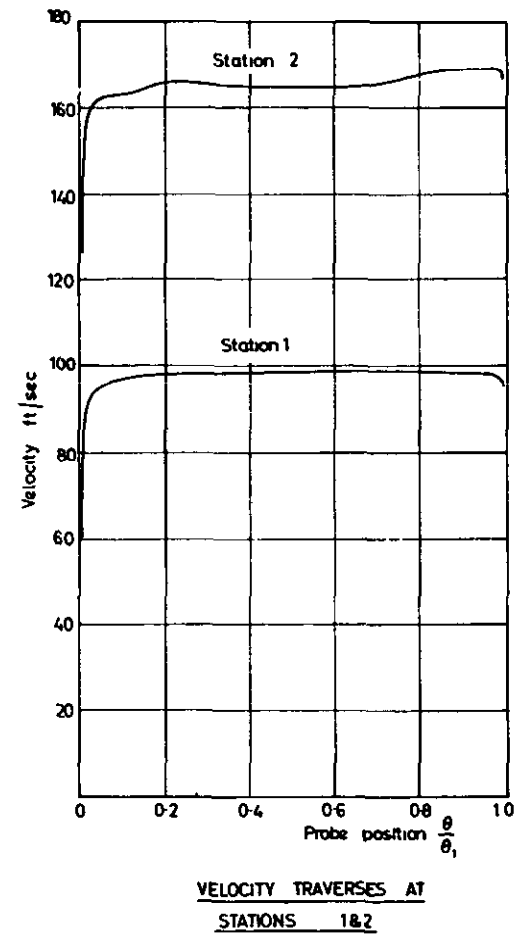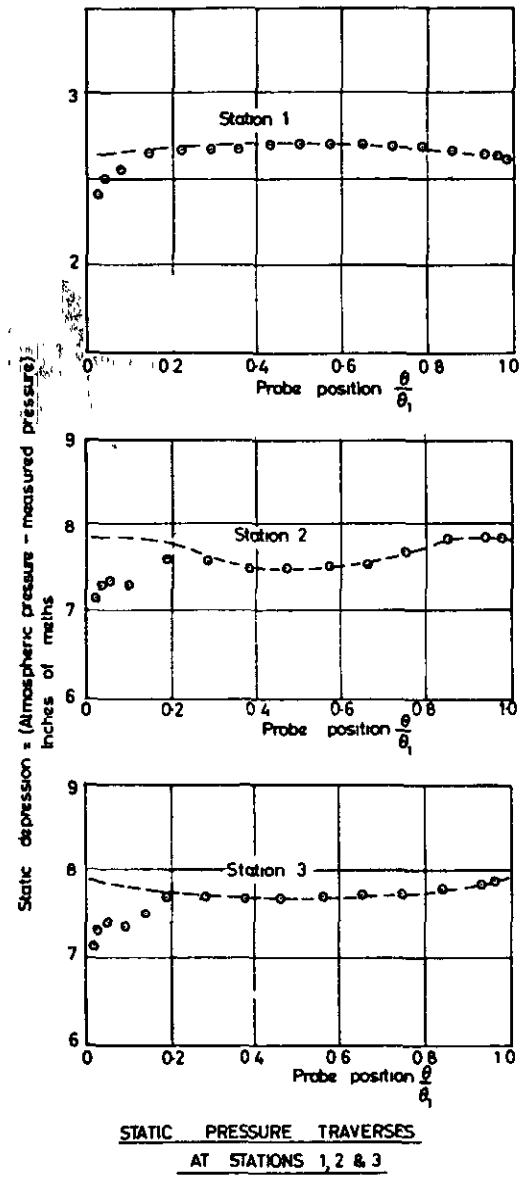
THE ENGLISH ELECTRIC COMPANY LIMITED	STATIC PRESSURE & VELOCITY	Date	March 1963
MECHANICAL ENGINEERING LABORATORY	TRAVERSES AT INLET & OUTLET	Drawing No	R20172 − 3192
WHETSTONE	OF CONICAL CONTRACTION	Report No.	W/M (2A) p.74
		Figure Sheet No 12	

FIG.13

Full curve ~ inlet station 1
Dashed curve ~ Outlet station 3 predicted
o ~ Outlet station 3 experiment

Axial velocity $\dfrac{u}{U}$

Probe position θ/θ_1
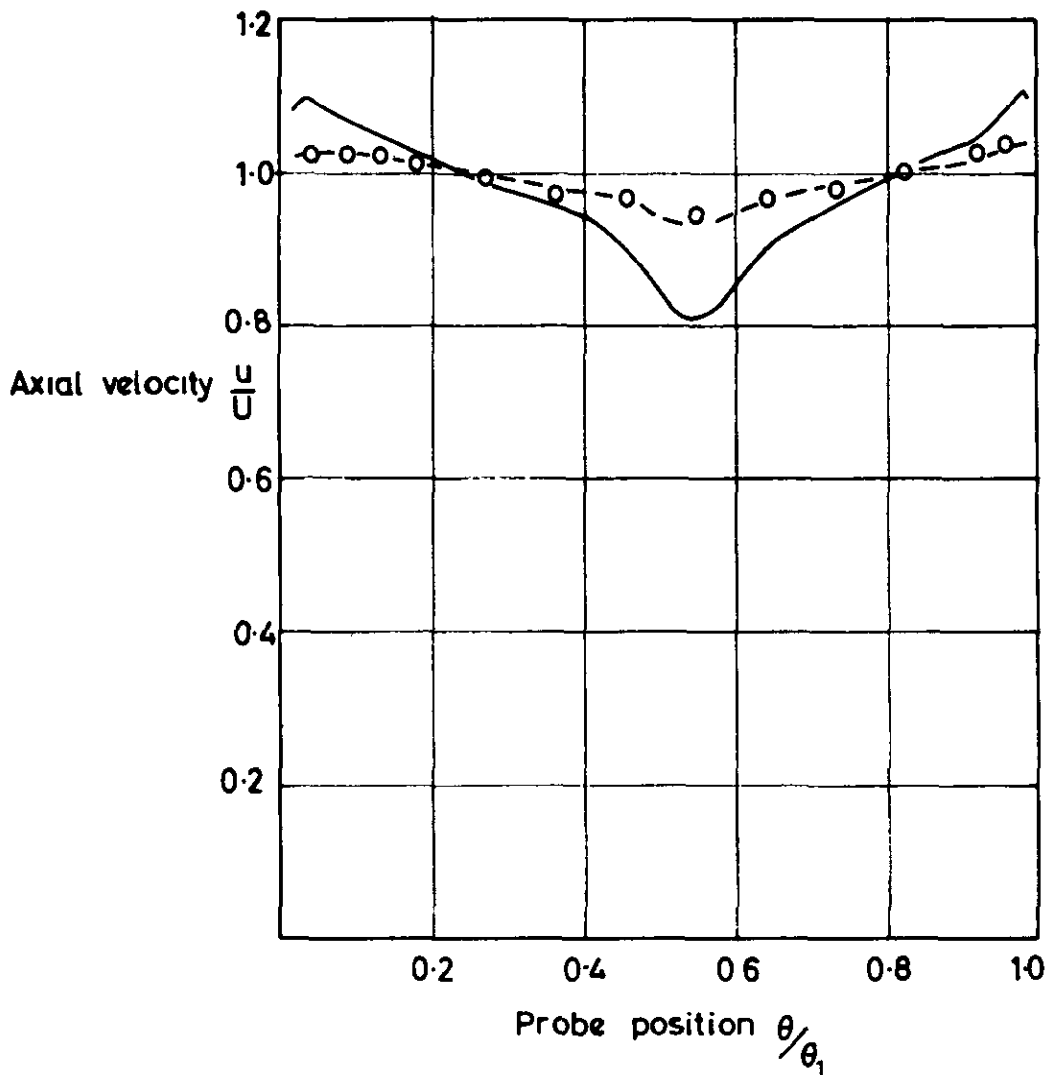
NON-UNIFORM FLOW THROUGH A CONICAL CONTRACTION

$2\theta = 20°24' \lambda = 0.59$

FIG.14

Station 1 ~ full curve

Station 2 ~ dashed curve
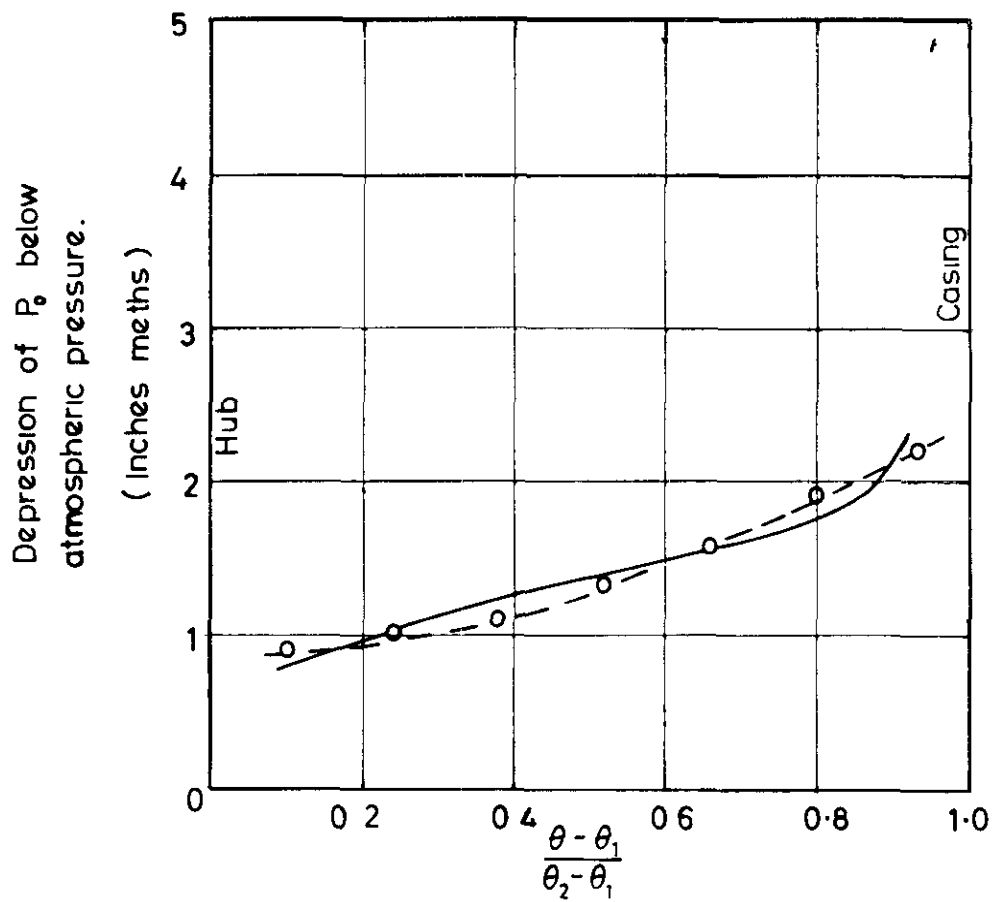
TOTAL   PRESSURE   AT   INLET   AND   OUTLET   OF

CONICAL   ANNULUS   WITH   SMALL   SWIRLING   VELOCITY.
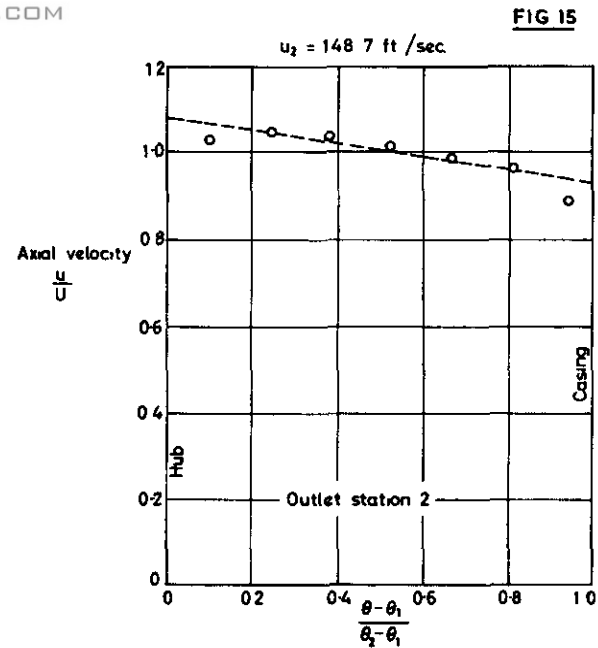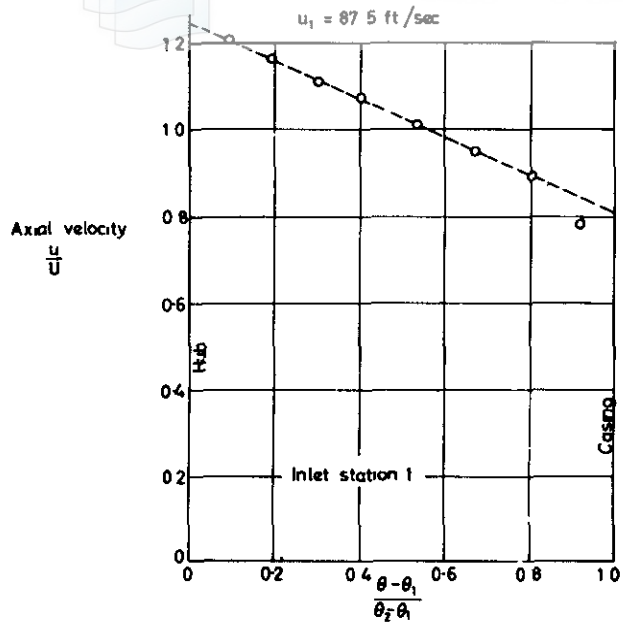
FIG 15

FIG 15 (a) AXIAL VELOCITY AT STATIONS 1 & 2
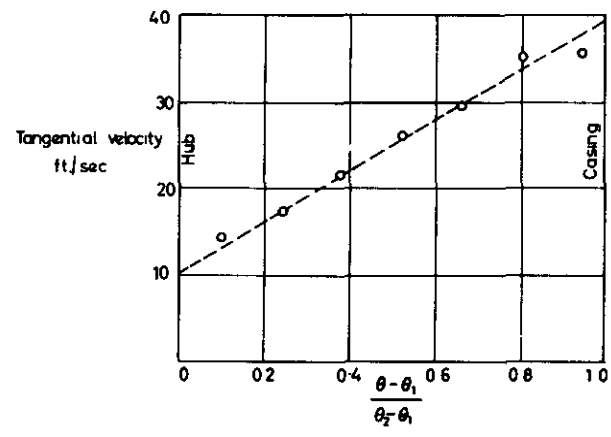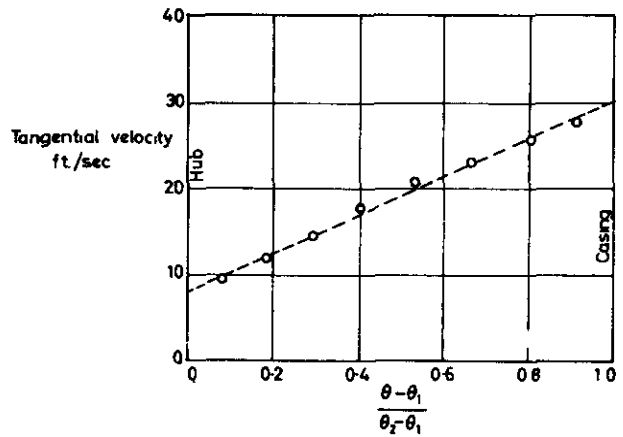
FIG 15 (b) SWIRLING VELOCITY AT STATIONS 1 AND 2

o Experimental points
Dashed curve ~ theory

THEORETICAL AND EXPERIMENTAL
VELOCITY COMPONENTS AT INLET
AND OUTLET OF CONICAL ANNULUS WITH
SMALL SWIRLING VELOCITIES

FIG.16

Station 1

Duct inlet

Hub

Casing

$$\frac{\theta - \theta_1}{\theta_2 - \theta_1}$$

Loss of total pressure - inches of meths

Station 2

Just upstream of blades

Hub

Casing

$$\frac{\theta - \theta_1}{\theta_2 - \theta_1}$$
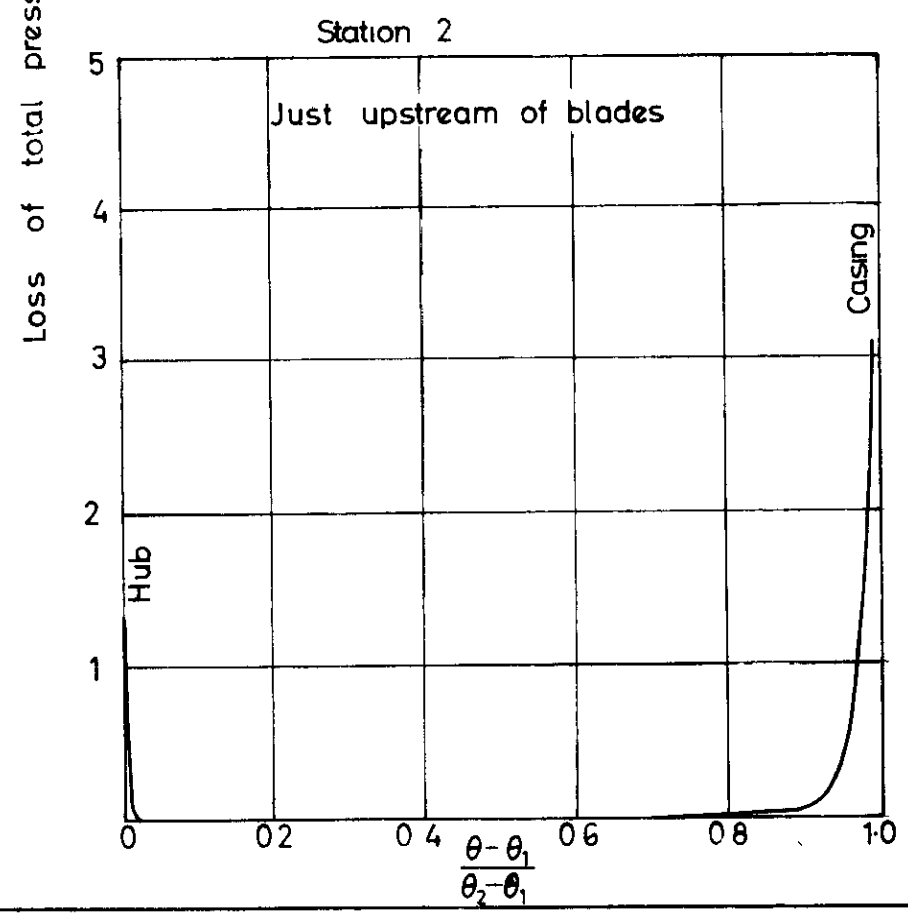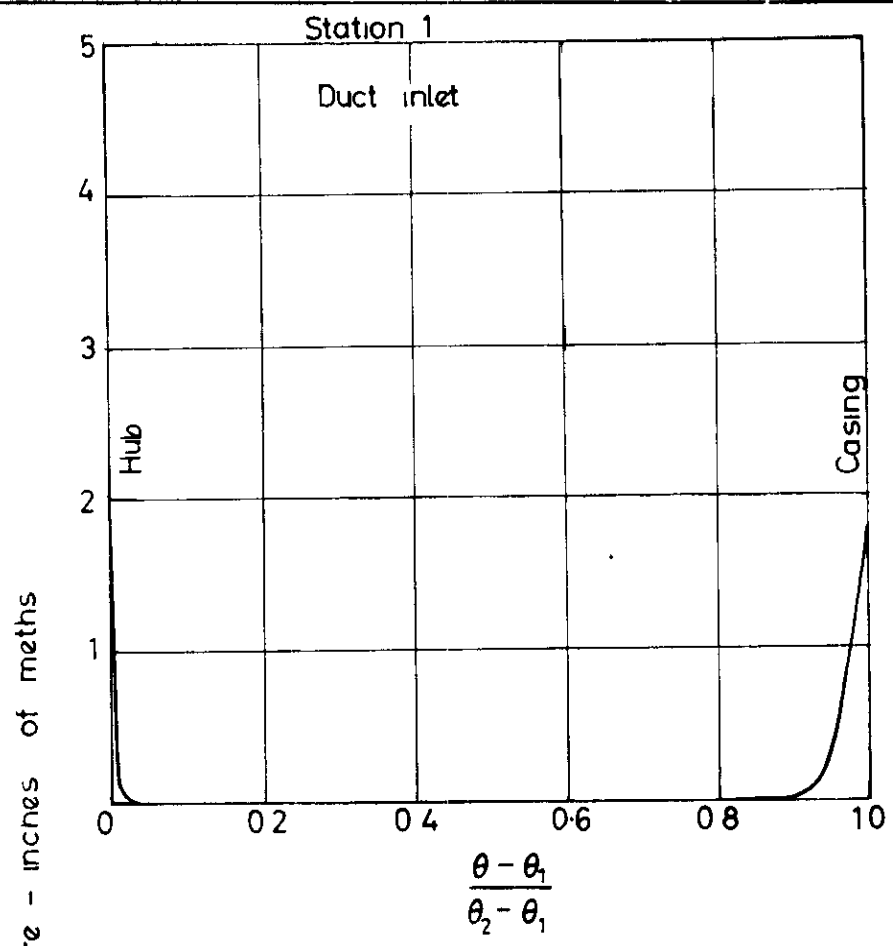
BOUNDARY LAYER TRAVERSES AT STATIONS 1 & 2

OF CONICAL ANNULAR DUCT.

FIG.17

Axial velocity
~ Ft/sec

Axial velocity variation
entirely due to static
pressure gradient except
in boundary layer regions.
i.e total pressure is constant.

Station 2

Station 1

Hub

Casing

$$\frac{\theta - \theta_1}{\theta_2 - \theta_1}$$
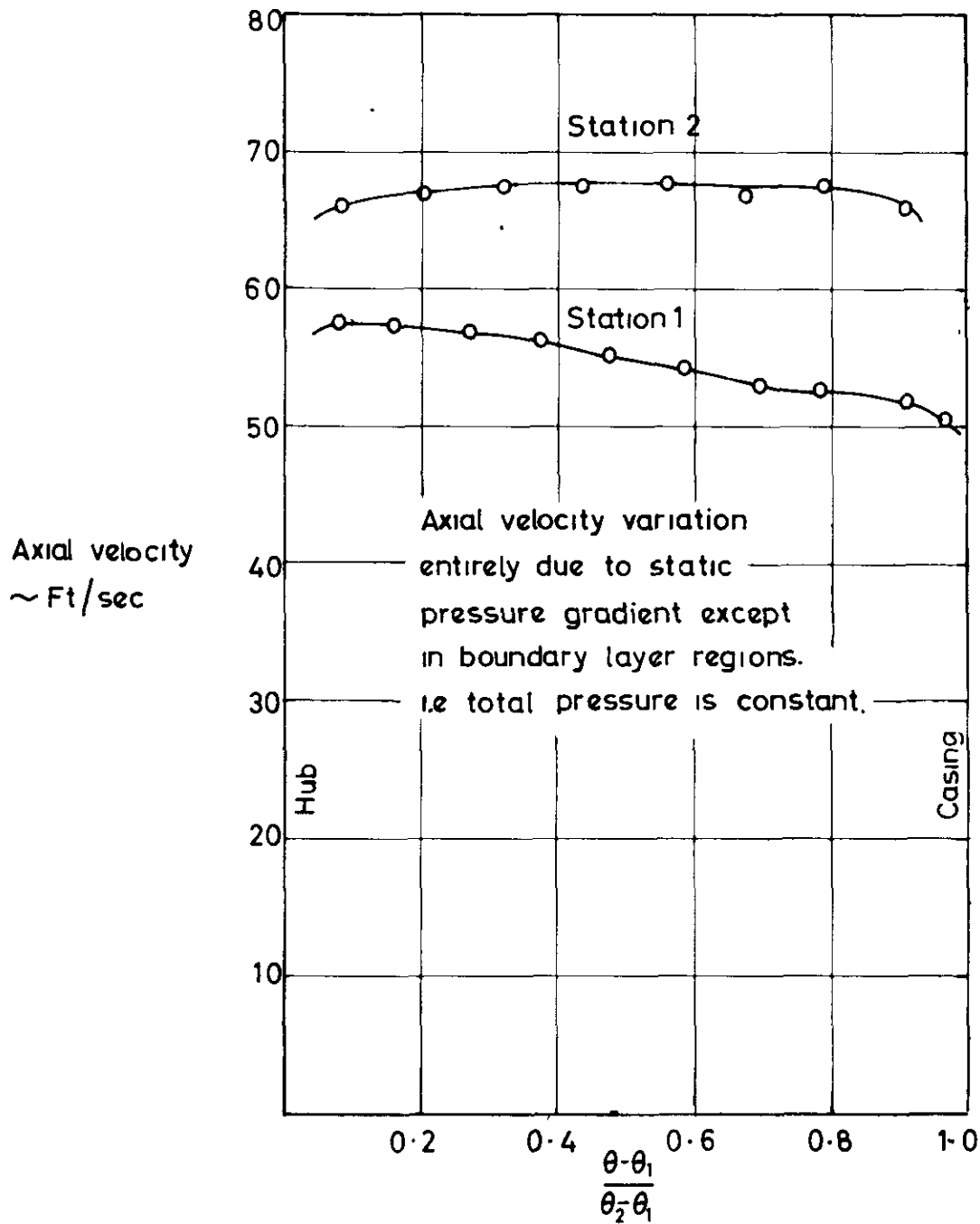
AXIAL VELOCITY PROFILES AT

STATIONS 1 AND 2 UPSTREAM OF FREE -VORTEX

CASCADE IN CONICAL ANNULUS

FIG. 18

Dashed curve shows design angles
at equivalent radial position in cylindrical flow
o— angles measured with non uniform Inflow
full curve- angles measured with uniform inflow.

Swirl angle α°

Hub

Casing

$$\frac{\theta - \theta_1}{\theta_2 - \theta_1}$$
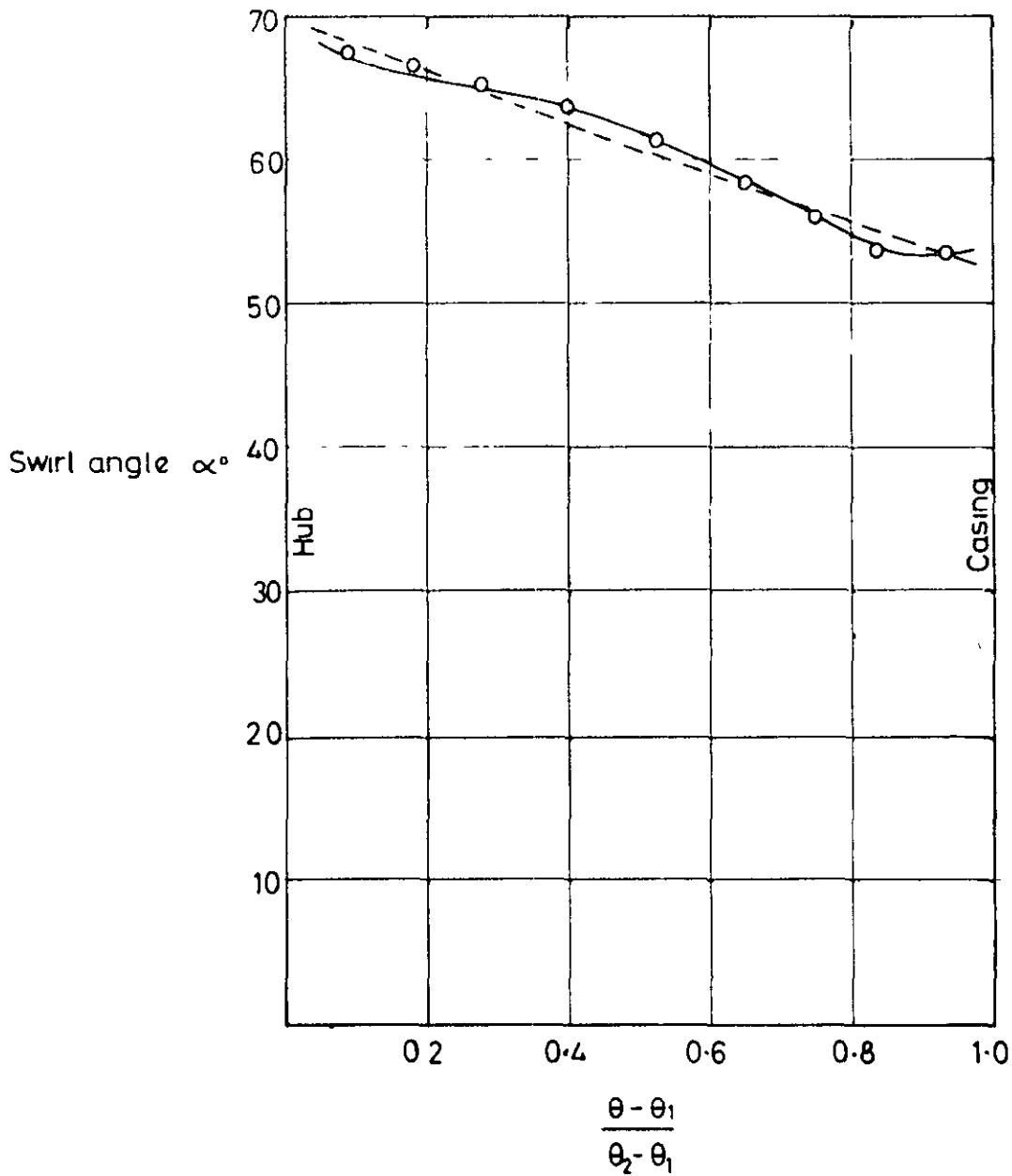
SWIRL ANGLES AT STATION 3 DOWNSTREAM OF FREE VORTEX

CASCADE IN CONVERGING CONICAL ANNULUS

FIG. 19

Curves (a) & (b) show design free vortex components.
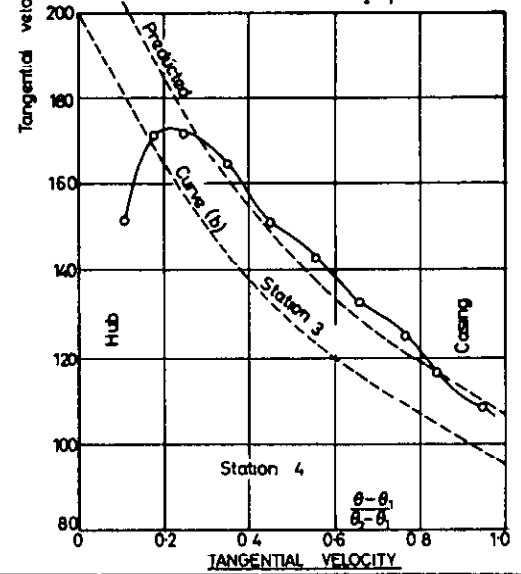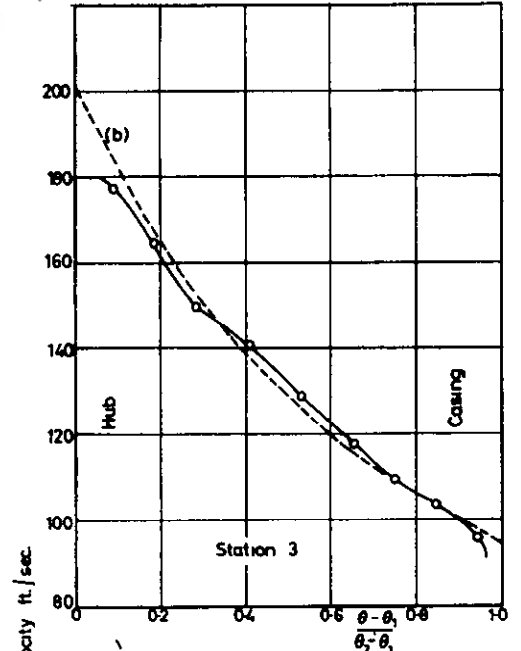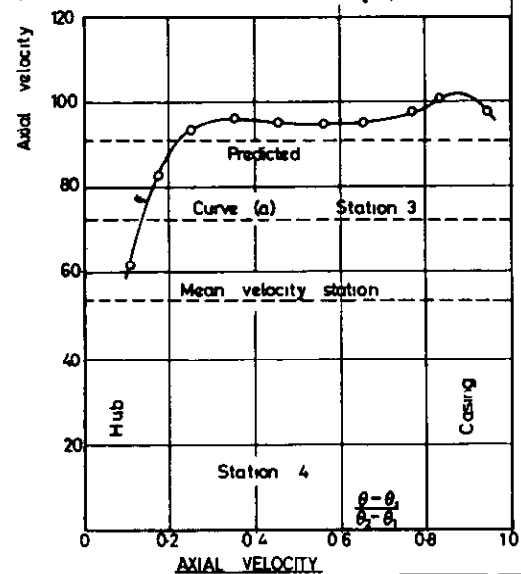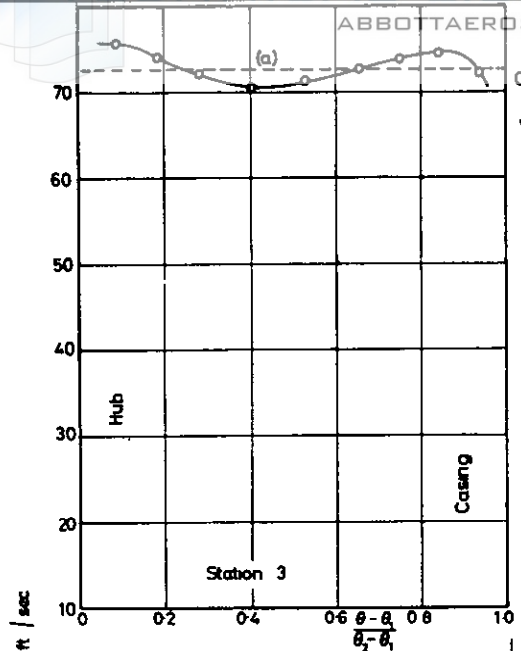
VELOCITY COMPONENTS DOWNSTREAM
OF FREE VORTEX CASCADE IN A
CONVERGING CONICAL ANNULUS

FIG.20

Station 2

Station 4

$\dfrac{\theta - \theta_1}{\theta_2 \theta_1}$
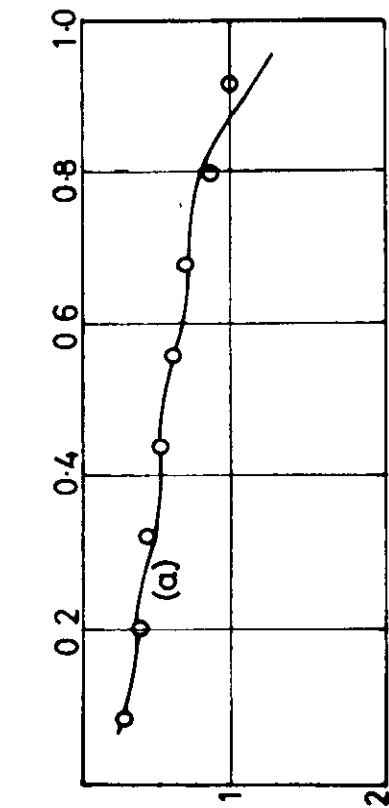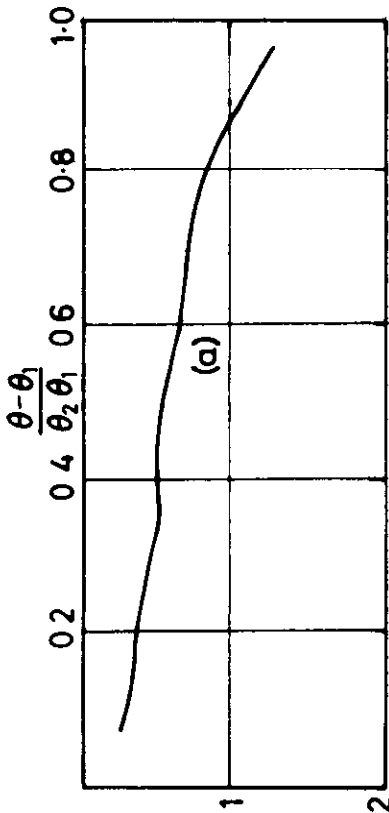
Station 1 inlet

Curve (a) shows inlet distribution of P_0 superimposed on plots at other stations for comparison
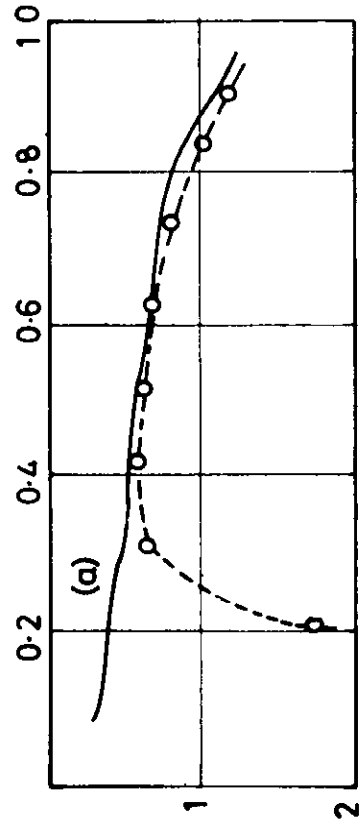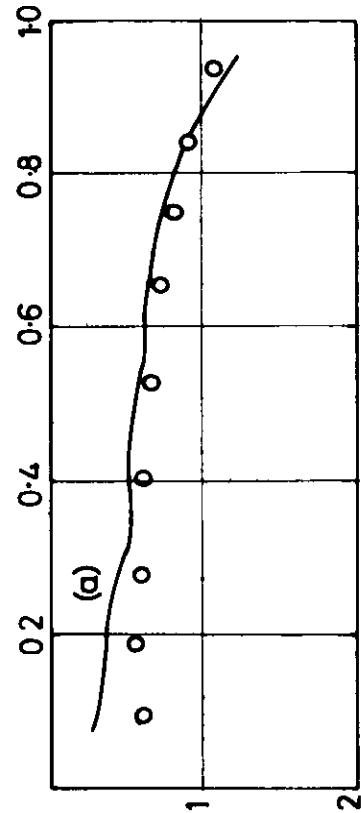
Station 3

(Room pressure—total pressure) inches of meths

TOTAL PRESSURE PROFILES IN CONICAL

ANNULUS WITH FREE VORTEX BLADES
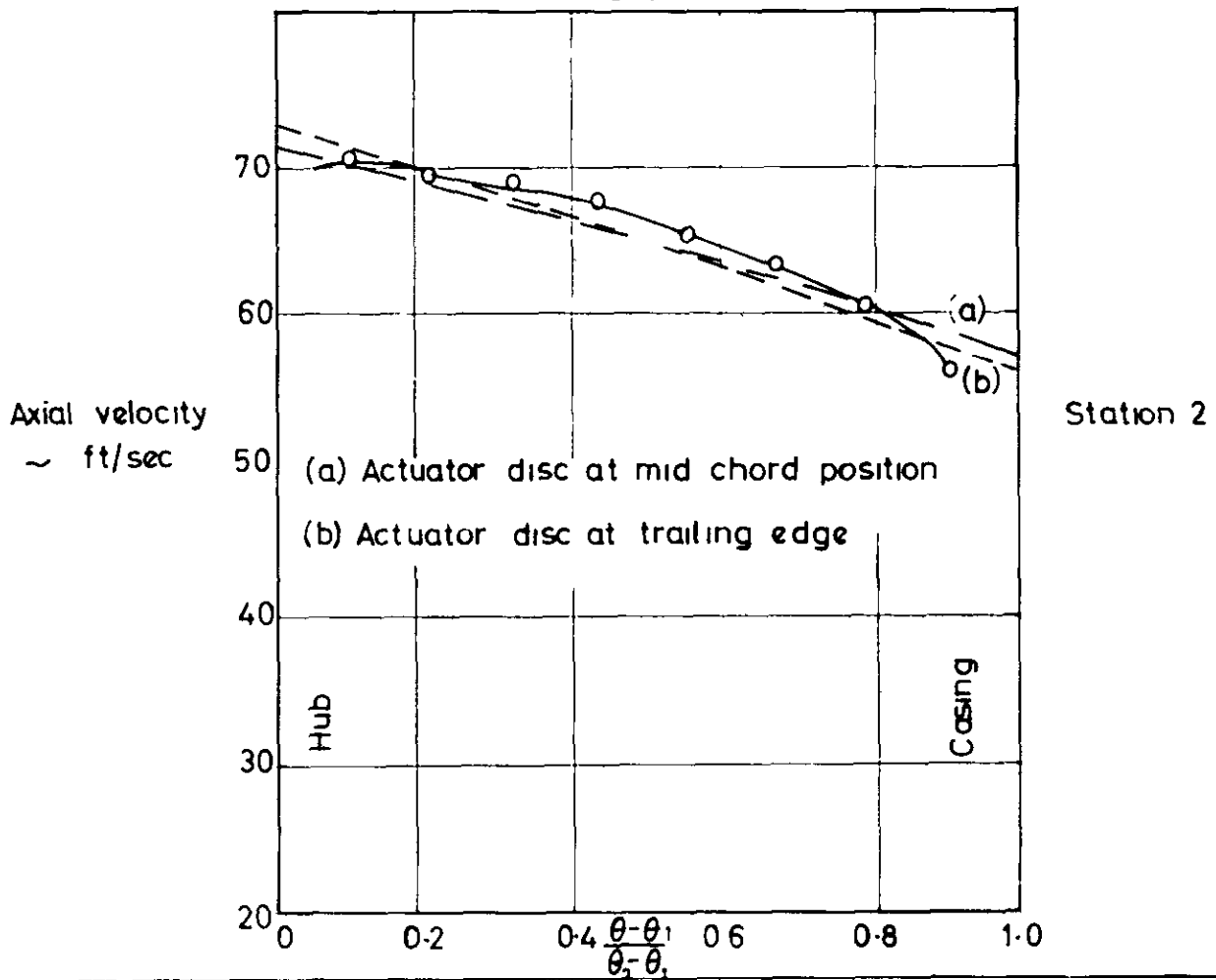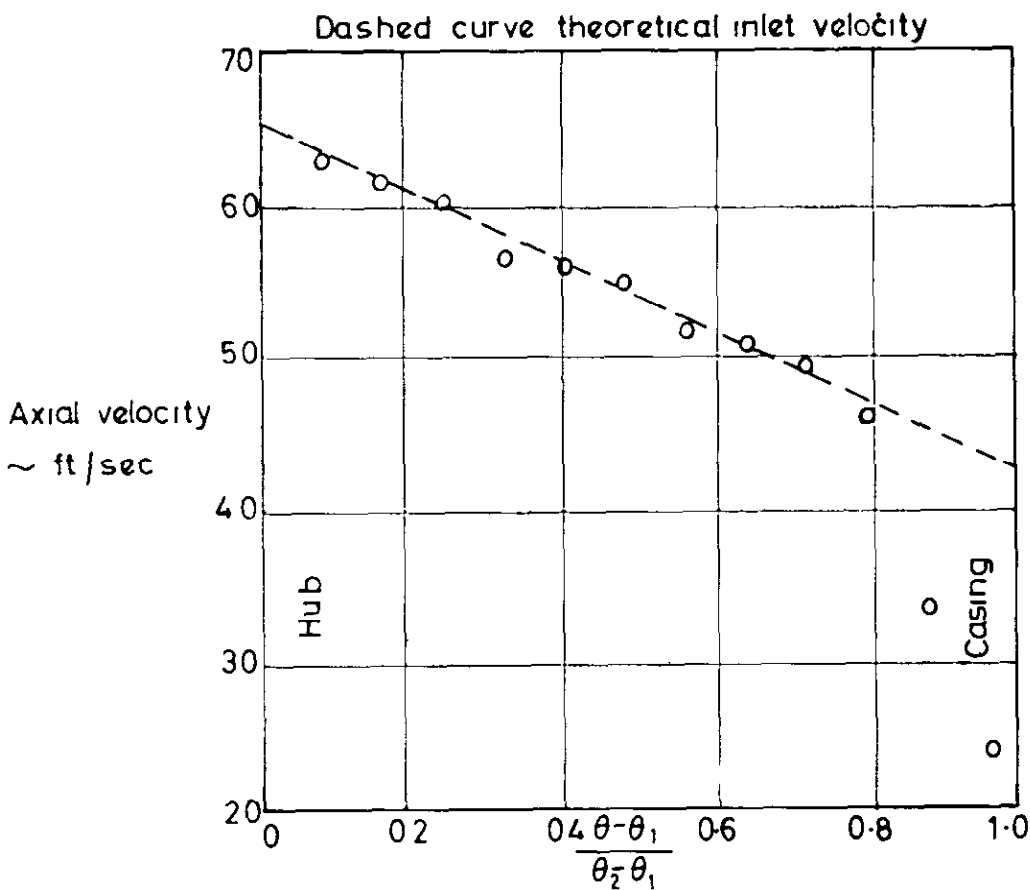
AXIAL VELOCITY PROFILES AT STATIONS 1 AND 2

UPSTREAM OF FREE VORTEX ANNULAR CASCADE IN

CONICAL ANNULUS WITH GRADIENT OF TOTAL PRESSURE
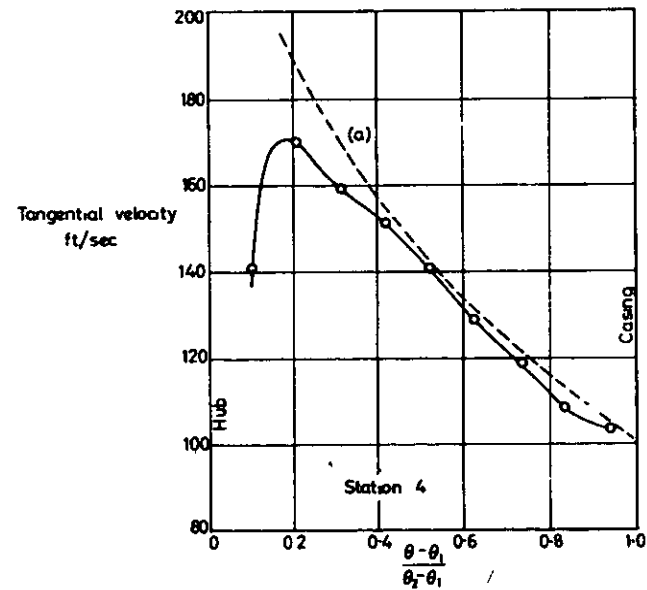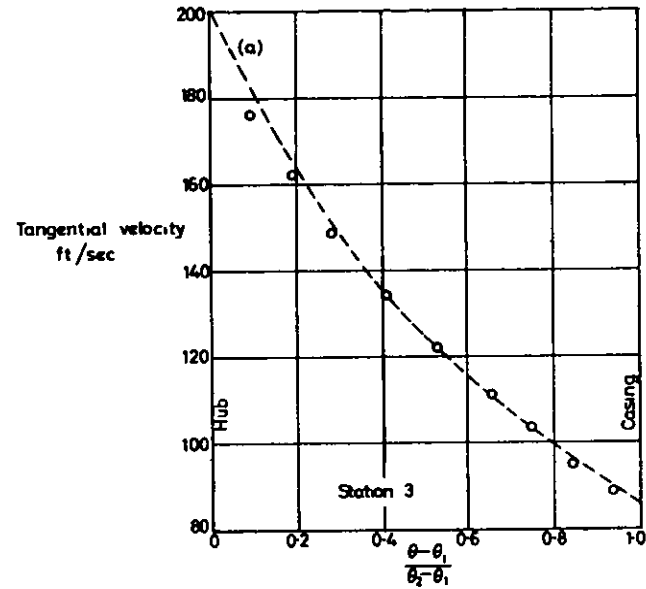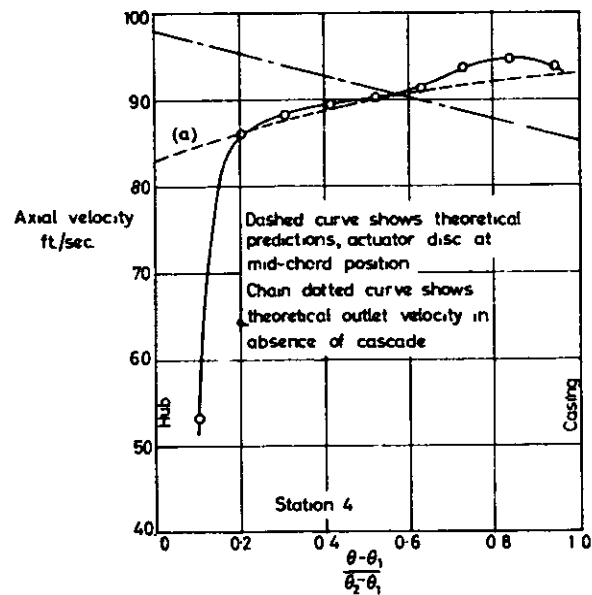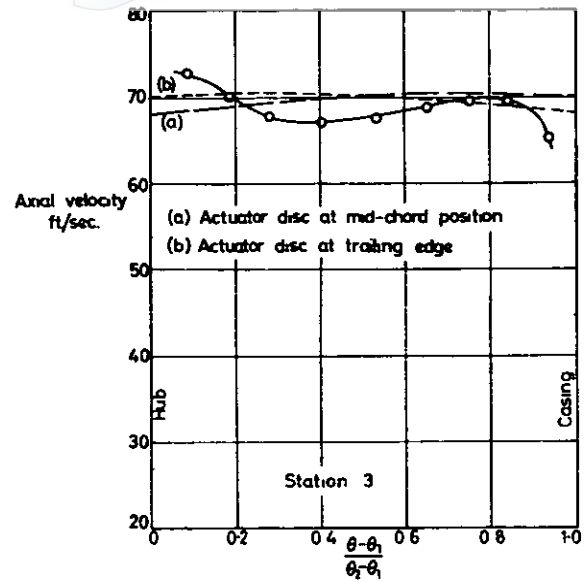
FIG. 22

VELOCITY COMPONENTS DOWNSTREAM OF
FREE VORTEX ANNULAR CASCADE IN
CONICAL ANNULUS WITH NON-UNIFORM
INLET STAGNATION PRESSURE

Top-left graph: Axial velocity ft/sec. vs $\frac{\theta - \theta_1}{\theta_2 - \theta_1}$, Station 3
(a) Actuator disc at mid-chord position
(b) Actuator disc at trailing edge

Top-right graph: Tangential velocity ft/sec vs $\frac{\theta - \theta_1}{\theta_2 - \theta_1}$, Station 3

Bottom-left graph: Axial velocity ft/sec. vs $\frac{\theta - \theta_1}{\theta_2 - \theta_1}$, Station 4
Dashed curve shows theoretical predictions, actuator disc at mid-chord position
Chain dotted curve shows theoretical outlet velocity in absence of cascade

Bottom-right graph: Tangential velocity ft/sec vs $\frac{\theta - \theta_1}{\theta_2 - \theta_1}$, Station 4

o Swirl angles with non-uniform stagnation pressure

The full curve indicates swirl angles with
constant stagnation pressure

o Swirl angle estimated from measurements at station 3

Dashed curve shows theoretical mean swirl angles at the
cascade given by $\tan \alpha_m = 3\cdot3\theta - 1\cdot28$
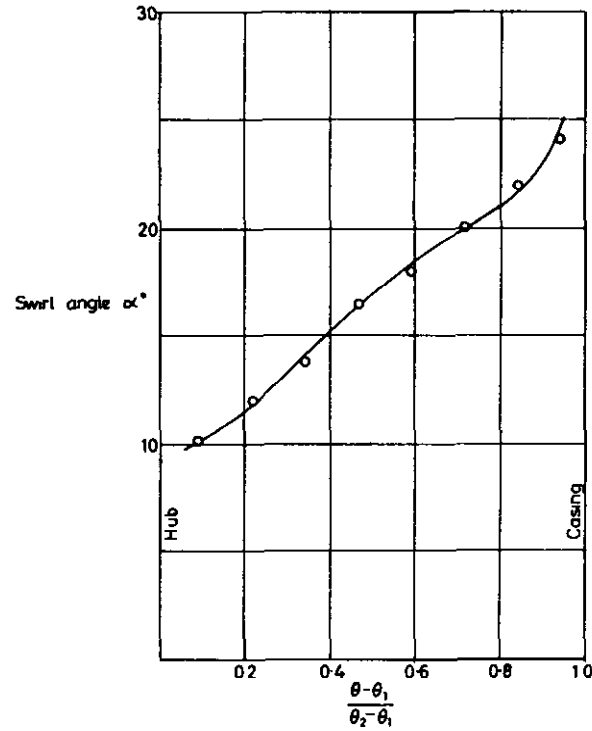
FIG 23(a) SWIRL ANGLES AT STATION 3

NEAR BLADE TRAILING EDGES
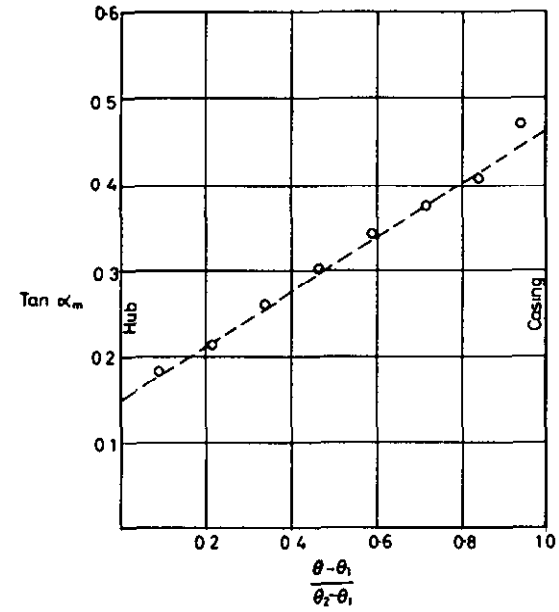
FIG 23(b) TANGENT OF SWIRL ANGLES AT THE ACTUATOR DISC

ESTIMATED FROM THE MEASUREMENTS

SWIRL ANGLES MEASURED AT STATION 3
AND ESTIMATED VALUES AT ACTUATOR
DISC REPRESENTING COMPRESSOR
INLET GUIDE VANES

FIG. 24

Static depression ~ inches meths

Velocity ~ ft / sec
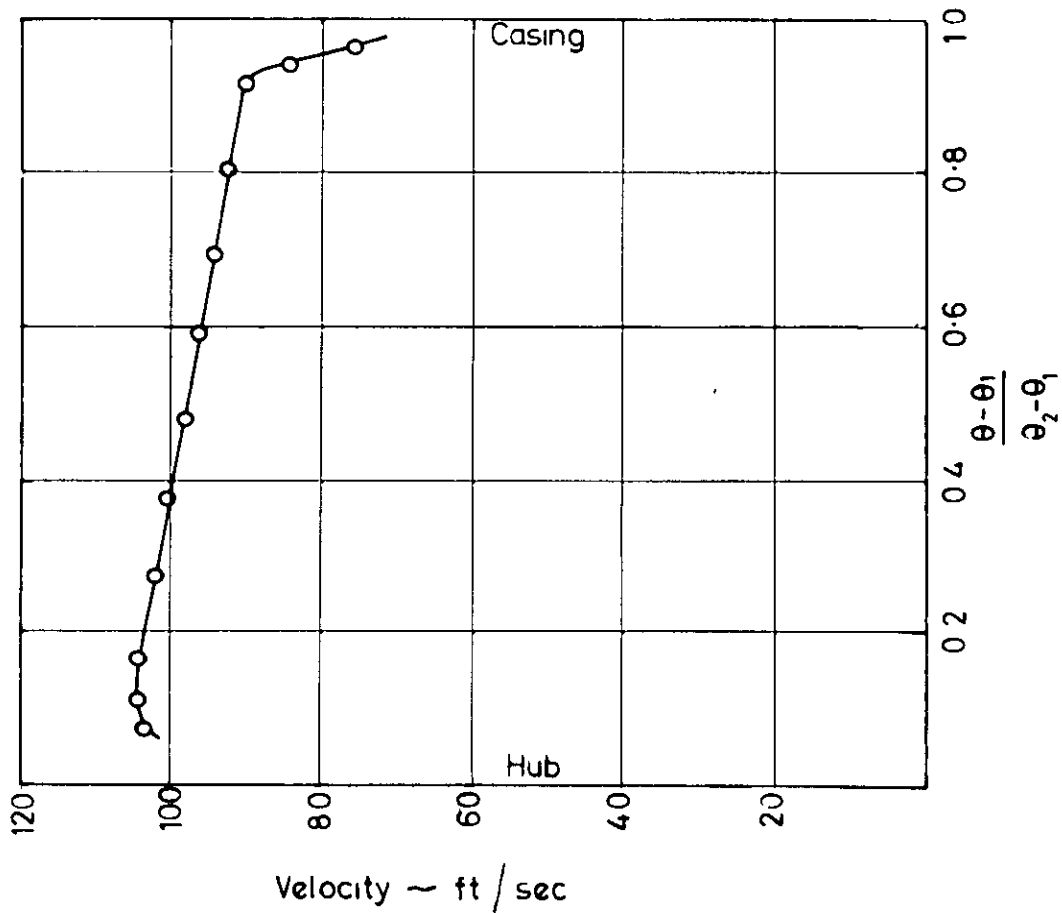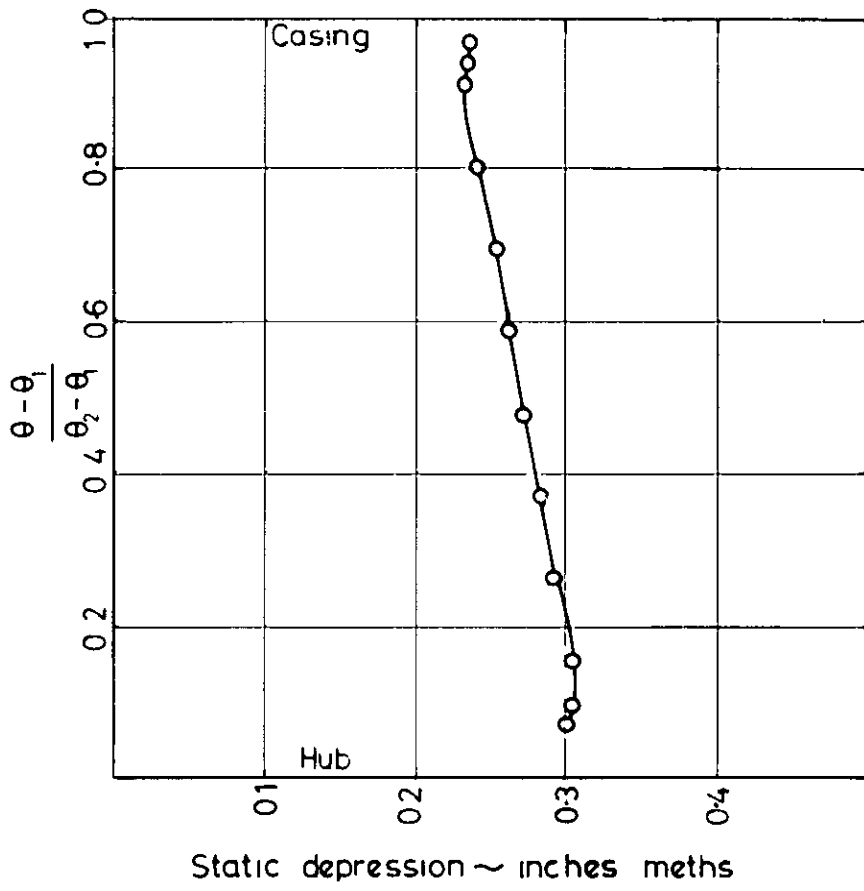
VELOCITY AND STATIC PRESSURE AT INLET - STATION 1

CONICAL ANNULUS WITH COMPRESSOR INLET GUIDE VANES

FIG.25

Solid curve — theory A uniform pressure at station 1

Dashed curve—theory B including pressure variation at station 1
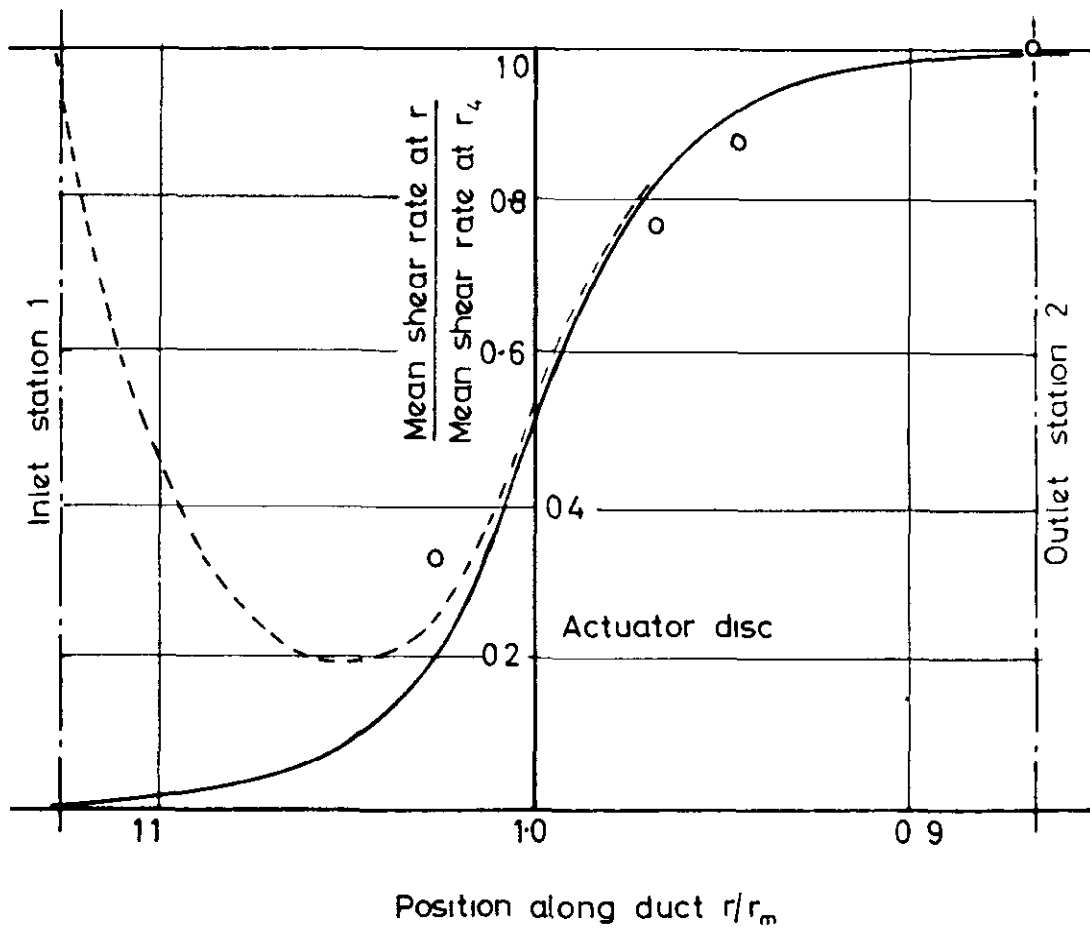
GROWTH OF AXIAL VELOCITY PERTURBATION (REPRESENTED

BY MEAN SHEAR RATE) WITH ACTUATOR CASCADE

PLACED AT $\frac{1}{3}$ OF BLADE CHORD FROM LEADING

EDGE ~ COMPARED WITH THEORY

FIG 26

Dashed curve shows theory with actuator
disc ⅓ of blade chord from leading edge

Dashed curve shows theoretical predictions,
fully corrected including non uniform pressure at inlet
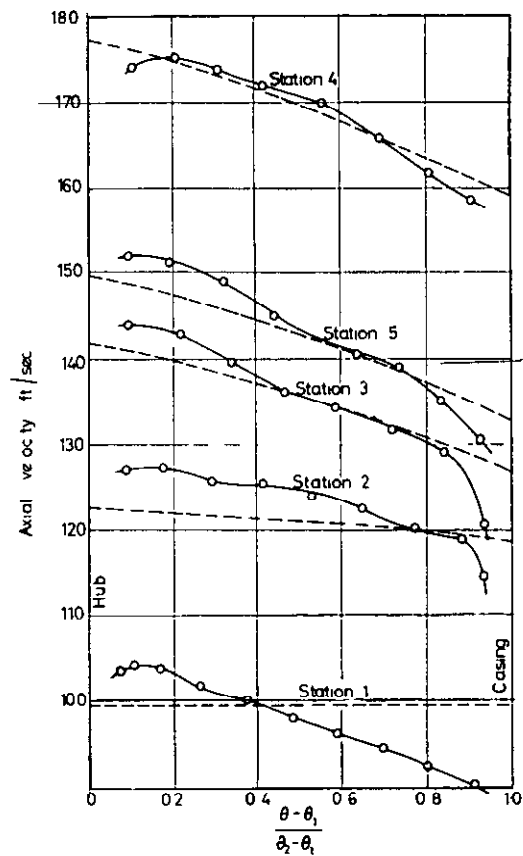
FIG 26(a) AXIAL VELOCITY THROUGH CONVERGING
DUCT WITH CONSTANT STAGNATION PRESSURE THEORY A
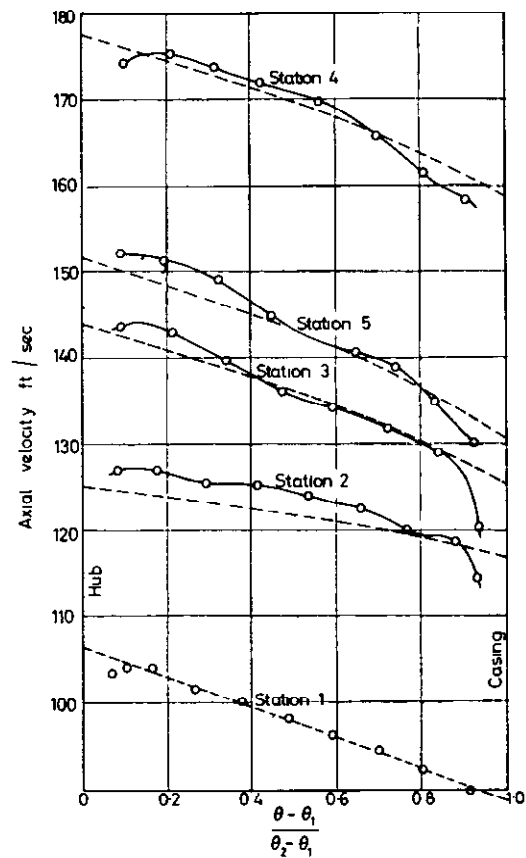
FIG 26(b) AXIAL VELOCITY THROUGH CONVERGING
DUCT WITH CONSTANT STAGNATION PRESSURE THEORY B

AXIAL VELOCITY THROUGH CONICAL
ANNULUS CONTAINING COMPRESSOR
INLET GUIDE VANES
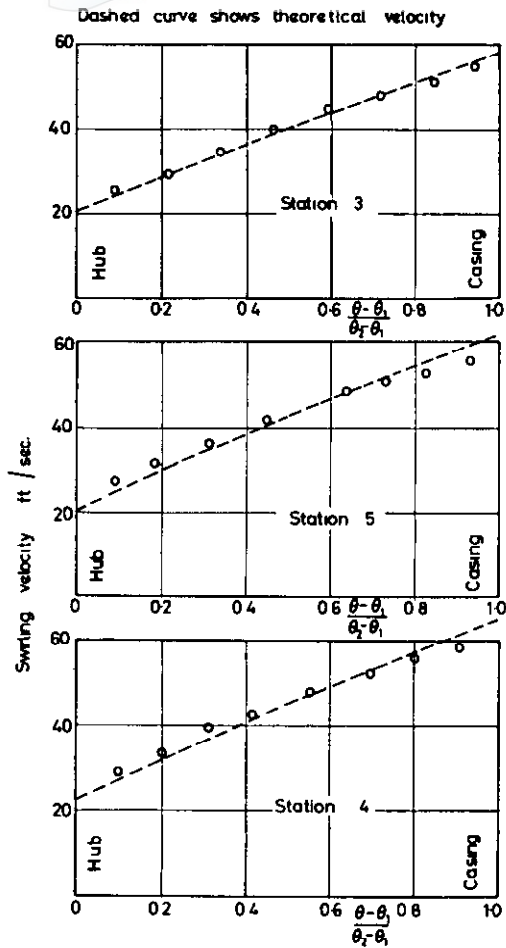
FIG 27

FIG 27(a) SWIRLING VELOCITY COMPONENT
AT STATIONS 3,4 & 5
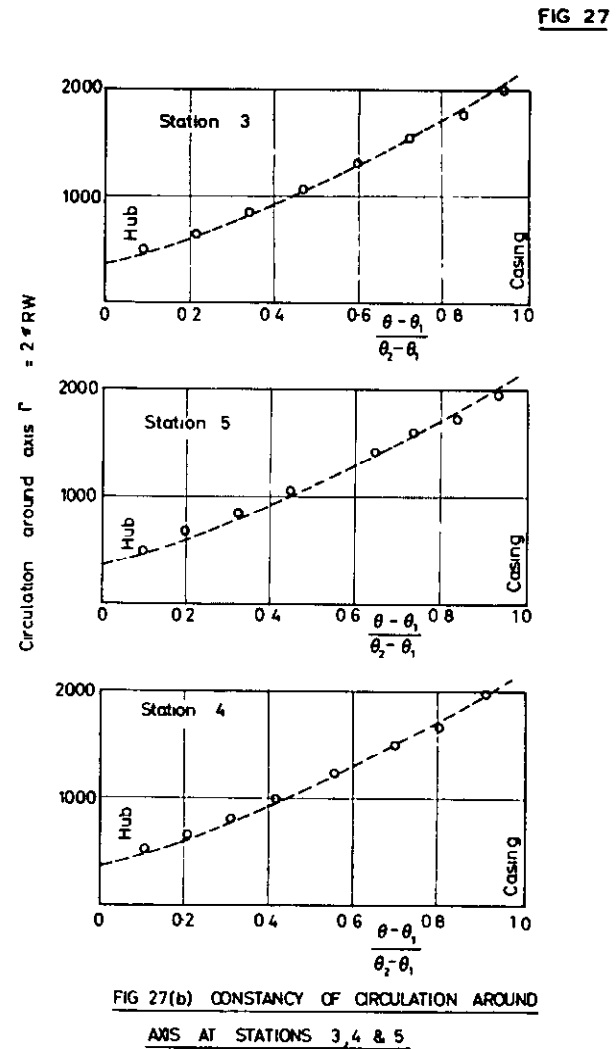
FIG 27(b) CONSTANCY OF CIRCULATION AROUND
AXIS AT STATIONS 3,4 & 5

SWIRLING VELOCITY & CIRCULATION
DISTRIBUTION DOWNSTREAM OF
COMPRESSOR INLET GUIDE VANES

FIG.28
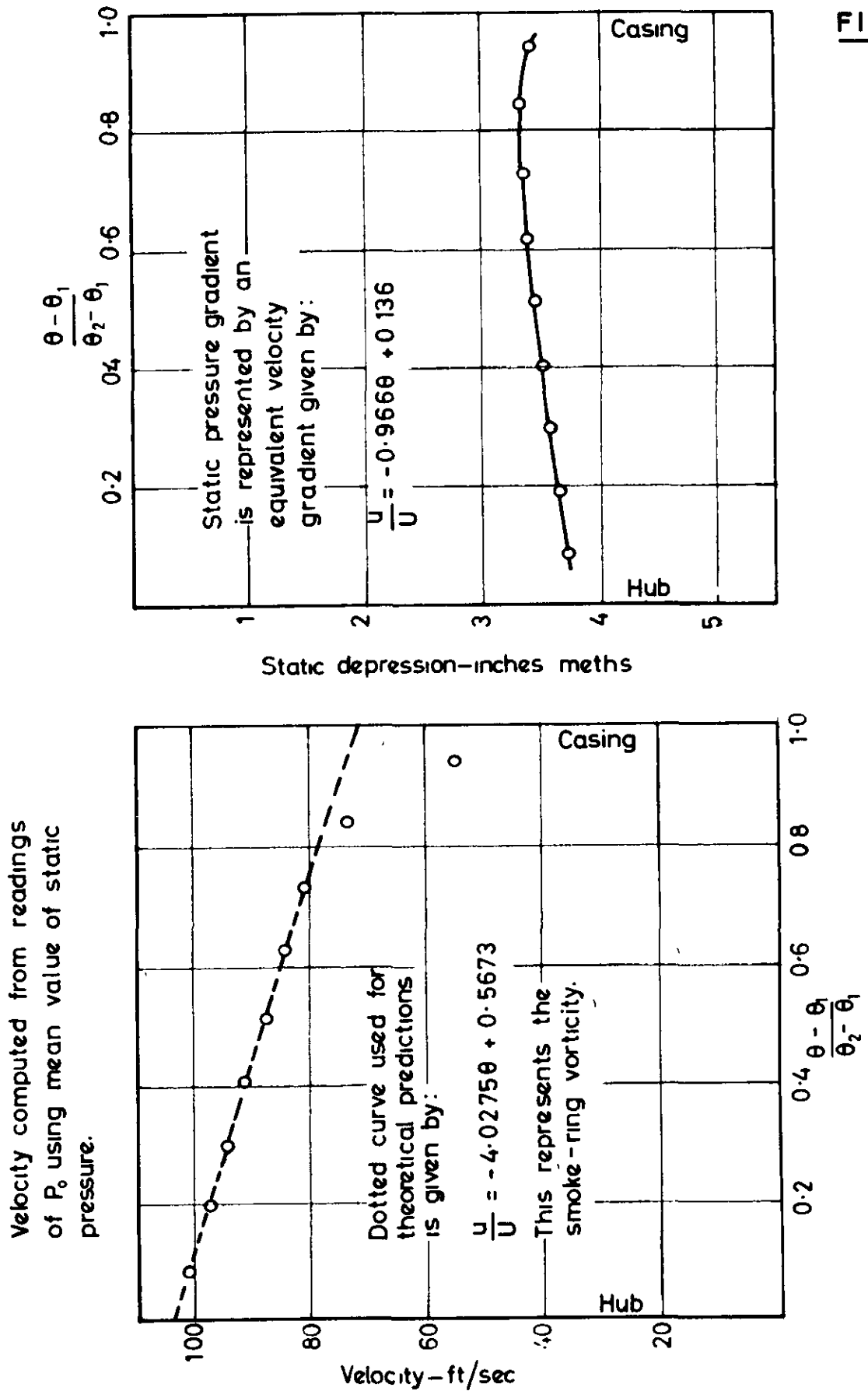
STATIC PRESSURE AND VELOCITY AT INLET STATION 1

CONVERGING ANNULUS WITH COMPRESSOR INLET GUIDE VANES

FIG 29

Axial velocity
~ ft/sec

Station 4

Station 5

Station 3

Station 2

Station 1

Hub

Casing

$$\frac{\theta - \theta_1}{\theta_2 - \theta_1}$$

Swirling velocity
~ ft/sec

Station 3

Hub

Casing

$$\frac{\theta - \theta_1}{\theta_2 - \theta_1}$$

Swirling velocity
~ ft/sec

Station 5

Hub

Casing

$$\frac{\theta - \theta_1}{\theta_2 - \theta_1}$$

Swirling velocity
~ ft/sec

Station 4

Hub

Casing

$$\frac{\theta - \theta_1}{\theta_2 - \theta_1}$$

Dashed curves show predicted velocities.
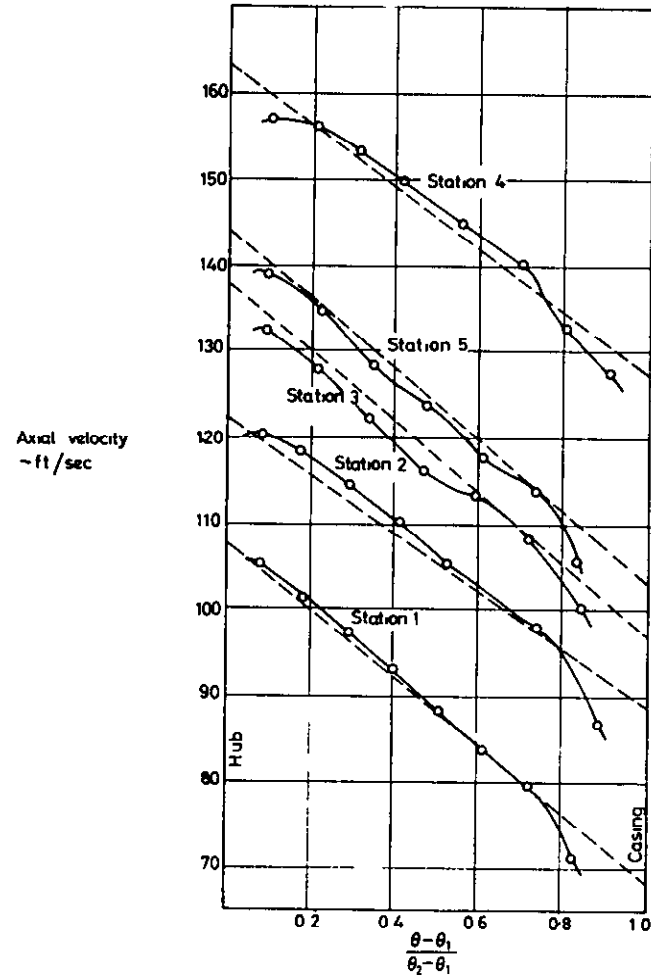
FIG 29 (a) AXIAL VELOCITY COMPONENTS AT STATIONS 1 2 3 5 & 4
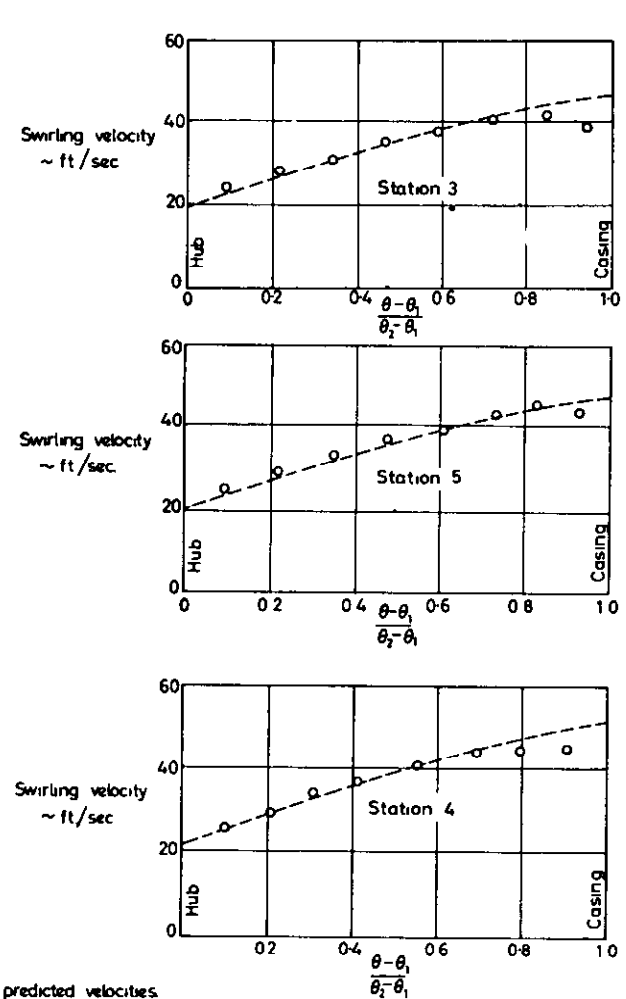
FIG 29 (b) SWIRLING VELOCITY COMPONENT AT STATIONS 3 4 & 5

AXIAL AND SWIRLING VELOCITY COMPONENTS
WITHIN CONICAL DUCT CONTAINING
COMPRESSOR INLET GUIDE VANES WITH
NON-UNIFORM INLET STAGNATION PRESSURE

FIG.30
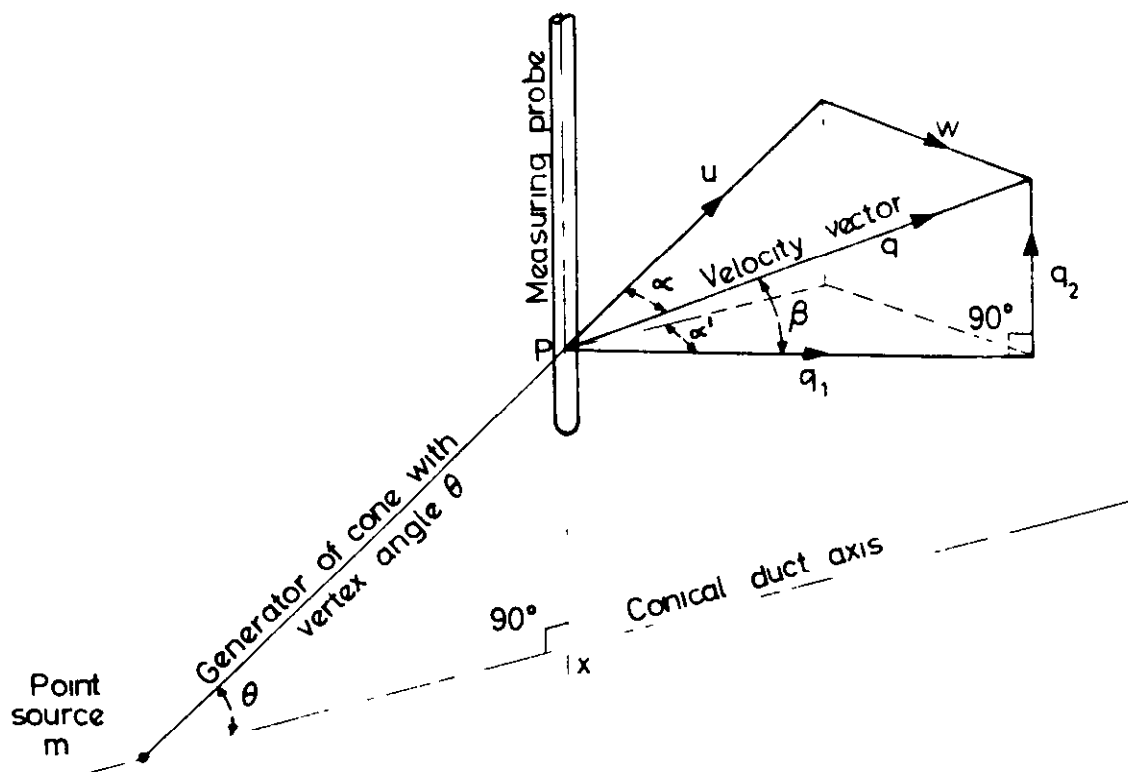
INTERSECTION OF MEASURING PROBE & VELOCITY

VECTOR q IN CONICAL SWIRLING FLOW.

A.R.C. C.P. No.766
October, 1963
R. I. Lewis

ANNULAR CASCADE EXPERIMENTAL INVESTIGATIONS OF CONICAL
ACTUATOR DISC THEORY AND OF NON-UNIFORM FLOW THROUGH
PLANE WALLED DIVERGING OR CONVERGING DUCTS

A description is given of wind-tunnel experimental investigations of
rotational flows through diffusers and contractions. The purpose of the
investigations was to test the accuracy of a theory previously derived for
two-dimensional plane walled diverging or converging ducts and of actuator
disc theory for conical annuli. Conical flow tests were made in one case
with a free vortex blade row of large deflection. Other tests were made
with an axial compressor inlet guide vane nozzle generating a small
swirling velocity distribution close to solid rotation. Particular
attention is drawn to the separate influences exerted by two vorticity
components originating from gradients of stagnation pressure and of fluid
angular momentum.

S.O. Code No. 23-9015-66